



Aalborg Universitet

AALBORG UNIVERSITY  
DENMARK

## Utilizing computational modeling in the design of a new electrode for preferential activation of small cutaneous nerve fibers

Poulsen, Aida Hejlskov

*Publication date:*  
2021

*Document Version*  
Publisher's PDF, also known as Version of record

[Link to publication from Aalborg University](#)

*Citation for published version (APA):*  
Poulsen, A. H. (2021). *Utilizing computational modeling in the design of a new electrode for preferential activation of small cutaneous nerve fibers*. Aalborg Universitetsforlag. Aalborg Universitet. Det Sundhedsvidenskabelige Fakultet. Ph.D.-Serien

### General rights

Copyright and moral rights for the publications made accessible in the public portal are retained by the authors and/or other copyright owners and it is a condition of accessing publications that users recognise and abide by the legal requirements associated with these rights.

- Users may download and print one copy of any publication from the public portal for the purpose of private study or research.
- You may not further distribute the material or use it for any profit-making activity or commercial gain
- You may freely distribute the URL identifying the publication in the public portal -

### Take down policy

If you believe that this document breaches copyright please contact us at [vbn@aub.aau.dk](mailto:vbn@aub.aau.dk) providing details, and we will remove access to the work immediately and investigate your claim.



**UTILIZING COMPUTATIONAL  
MODELING IN THE DESIGN OF A NEW  
ELECTRODE FOR PREFERENTIAL  
ACTIVATION OF SMALL CUTANEOUS  
NERVE FIBERS**

**BY  
AIDA HEJLSKOV POULSEN**

DISSERTATION SUBMITTED 2021



**AALBORG UNIVERSITY**  
DENMARK



**UTILIZING COMPUTATIONAL  
MODELING IN THE DESIGN OF A NEW  
ELECTRODE FOR PREFERENTIAL  
ACTIVATION OF SMALL CUTANEOUS  
NERVE FIBERS**

by

Aida Hejlskov Poulsen

Dissertation submitted 2021

Dissertation submitted: June 2021

PhD supervisor: Associate Prof. Carsten Dahl Mørch,  
Aalborg University

Assistant PhD supervisors: Prof. Ole Kæseler Andersen,  
Aalborg University  
Assistant Prof. Jenny Tigerholm,  
Aalborg University

PhD committee: Professor Johannes J. Struijk (chair)  
Aalborg University  
Professor Ulf Baumgärtner  
Medical School Hamburg (MSH)  
Director Thierry Keller  
TECNALIA, Health Division

PhD Series: Faculty of Medicine, Aalborg University

Department: Department of Health Science and Technology

ISSN (online): 2246-1302

ISBN (online): 978-87-7210-957-2

Published by:  
Aalborg University Press  
Kroghstræde 3  
DK – 9220 Aalborg Ø  
Phone: +45 99407140  
aauf@forlag.aau.dk  
forlag.aau.dk

© Copyright: Aida Hejlskov Poulsen

Printed in Denmark by Rosendahls, 2021



## **CV**

### **AIDA HEJLSKOV POULSEN**

Aida has obtained a B.Sc. and a M.Sc. in Biomedical Engineering and Informatics from Aalborg University, Denmark. Subsequent to her master's degree, she enrolled as a Ph.D. fellow working at the Center for Neuroplasticity and Pain (CNAP) under the main supervision of Associate professor Carsten Dahl Mørch. Co-supervision was provided by Jenny Tigerholm and Ole Kæseler Andersen. The main part of Aida's research has involved computational modeling of electrical stimulation, with a focus on surface electrodes for activation and assessment of peripheral nerves. Aida has continuously disseminated the results of the Ph.D. work through poster presentations at the IASP world congress on pain (2018), the congress of the European Pain Federation EFIC (2019), and the annual Computational Neuroscience Meeting (2019). During her Ph.D. fellowship, she has additionally been involved with both teaching and supervision of biomedical engineering and medical students





# PREFACE

This PhD thesis provides a summary of the research conducted in the years from 2017 to 2021 at the Center for Neuroplasticity and Pain (CNAP), Department of Health Science and Technology, Aalborg University, Denmark. The project was financially supported by the Danish National Research Foundation (DNRF121).

The research of the present thesis aims at improving electrode designs for preferential small fiber activation by the use of a systematic computational modeling framework. The thesis is based on three scientific papers, of which two are published, and one is submitted for review. The first paper concerned the development and validation of a computational model of electrical stimulation of the human forearm. Subsequently, the second paper utilized the developed model to optimize electrode design parameters for small fiber activation. The results and knowledge obtained in the optimization study formed the basis of a new electrode design that was explored in the third paper using evoked potentials and psychophysical measurements.

Within the thesis, the methods and findings of the three papers are discussed in 5 chapters. The first chapter introduces the aim of the project as well as providing a brief introduction to the possible benefits of preferential electrical stimulation of small nociceptive fibers in the assessment of small fiber neuropathy. The second chapter will introduce the background knowledge of electrical stimulation and tissue properties, which are important, both for the understanding of the technique that is electrical stimulation and for the development and implementation of computational modeling of biological systems and electrical stimulation of tissues. The third chapter concerns the development and implementation of the computational model and the methods. The methods will include all the modeling methods used in the two published papers. Furthermore, the results of the model validation will be discussed. Chapter four will introduce a novel electrode design for small fiber activation, which was designed based on the results of the computational model. Additionally, chapter four will include the results of the third paper discussing the performance of the novel electrode design. Finally, concluding remarks and future perspectives of the presented work are provided in chapter five.



# ENGLISH SUMMARY

In recent years, small fiber neuropathy has become a well-recognized and increasing health care problem. Patients suffering from small fiber neuropathy are often experiencing debilitating pain. Small fiber neuropathy is relatively complex to diagnose, and treatment options are insufficient in most patients. Consequently, there is a need for clinical tools that can detect and assess small fiber dysfunction. Electrical stimulation could be a potential option, as it is widely used for large fiber assessment. However, conventional electrical stimulation targets large fibers, and nerve conduction studies display normal values in pure small fiber neuropathy. Consequently, recent research has been focusing on the development of specialized electrodes that will enable preferential activation of small fibers. At least six different electrodes have been developed and show promise in preferential small fiber activation. However, only low stimulation intensities are feasible, and the electrodes suffer from poor perception threshold reproducibility.

The present Ph.D. work aimed to investigate electrode design features and to design and test a novel electrode design for small fiber activation.

The thesis is based on three separate studies involving the development of a computational model and comparison of existing electrode designs, optimization, and experimental exploration of a novel electrode design. In the first study, a two-step model of the skin and innervating nerve fibers was implemented and used to compare five existing electrode designs. Furthermore, experimental data was collected to contribute to both electrode comparison and validation of the model. The experimental data corresponded well with the model simulations. The intra-epidermal needle design was most preferential towards small fibers as it displayed higher current densities in the vicinity of small fibers and a more limited current to deeper lying large fibers than the surface electrodes. Nevertheless, the effective area for which the electrode was small fiber preferential was smaller for the intra-epidermal design, wherefore practical considerations come into play, as this electrode needs to be placed in close proximity to a small nerve fiber ending to achieve preferentiality. The second study was an optimization study in which the validated model from the first study was used to optimize electrode dimensions for small fiber stimulation. Minimization of the electrode dimensions led to a substantial improvement of small fiber preferentiality. Accordingly, a small cathode made it possible to preferentially activate small fibers, while the small anode distance and dimensions increased the difference in small and large fiber activation threshold by limiting the current spread. The small contact area of the optimized electrode dimensions resulted in a smaller effective area of preferentiality. Consequently, electrode designs with multiple electrode anode-cathode pairs were considered to increase the probability of placing the electrode in the proximity of a nerve fiber

ending and utilize the phenomenon of spatial summation. From the optimization results, a novel electrode was designed, and in the third and final study, the new design was tested experimentally. The novel electrode design was compared to a regular patch electrode setup. Evoked potential predictions did display different patterns and latencies for the novel electrode and the patch, which could be due to differences in the activated fiber populations for the two electrodes. However, this was not quantified statistically. Consequently, some co-activation of large fibers may occur for stimulation with the novel electrode design. Nevertheless, the subjects rated the intensity of the stimuli to be higher and the quality to be sharper for the new electrode design, which, together with a lower perception threshold and longer reaction times, suggested small fiber activation. The sharpness and intensity of the sensation increased with increasing stimulus intensity, which might imply that the electrode is small fiber preferential even at relatively high intensities.

Throughout the work of this Ph.D., a systematic framework utilizing the benefits of computational modeling within the design phase of a novel stimulation electrode for small fiber activation was introduced. A novel planar single-use electrode was proposed as a further step towards a promising tool for assessing small fiber dysfunction.

# DANSK RESUMÉ

I de senere år er små-fiber neuropati blevet et mere og mere velkendt og stigende sundhedsproblem. Små-fiber neuropati er relativt komplekst at diagnosticere, og behandlingsmulighederne er utilstrækkelige for de fleste patienter, som ofte er plaget af stærke invaliderende smerter. Der er derfor et behov for kliniske værktøjer, der kan opdage og evaluere dysfunktion i de tynde nociceptive nervefibre. Elektrisk stimulering er en potentiel mulighed, som anvendes i vid udstrækning til evaluering af tykke nerve fibre, der blandt andet aktiveres ved trykpåvirkning. Konventionel elektrisk stimulation har dog den begrænsning at tykke fibre aktiveres ved lavere stimulerings intensitet end de små fibre, hvorfor resultaterne af en almindelig nerveledningsundersøgelse på en patient med små-fiber neuropati vil være inden for normalværdierne. Af denne årsag har nyere forskning fokuseret på udviklingen af specialiserede elektroder, der muliggør præferentiel aktivering af tynde nervefibre. Mindst seks forskellige elektroder er blevet udviklet med lovende resultater. Elektroderne er imidlertid begrænset til lave stimulationsintensiteter og har en ringe reproducerbarhed i henhold til estimering af perceptionstærskler.

Arbejdet under denne Ph.d. har derfor haft til formål at undersøge indflydelsen af elektrode-design og at designe og teste en ny elektrode til aktivering af nociceptorer.

Afhandlingen er baseret på tre separate studier, der involverede udviklingen af en fysiologisk model og sammenligning af eksisterende elektrodedesigns, samt optimering og eksperimentel udforskning af et nyt elektrodedesign. I det første studie blev en to-trins model af huden og nervefibrene i huden implementeret og anvendt til at sammenligne fem eksisterende elektrodedesigns. Desuden blev eksperimentelle data indsamlet for at bidrage til både elektrodesammenligning og validering af modellen. De eksperimentelle data var i god overensstemmelse med simuleringerne fra modellen. Det intra-epidermale elektrodedesign producerede den højeste strømtæthed i nærheden af de tynde nervefibre og genererede dermed den største forskel mellem aktivering af tynde og tykke nervefibre. På den anden side var det effektive område, for hvilket elektroderne aktiverede tynde fibre ved lavere intensitet end tykke fibre, mindst for det intra-epidermale design, hvormed praktiske overvejelser begynder at spille ind. Et lille areal med præferentiel aktivering af tynde fibre, betyder at elektroden skal placeres tæt på nervefibren. Andet studie var et optimeringsstudie, hvor den verificerede model fra første studie blev brugt til at optimere elektrodedimensioner. Minimering af elektrodedimensionerne førte til en væsentlig forbedring for aktivering af tynde nervefibre. Et lille katodeareal gjorde det muligt at aktivere tynde fibre ved lavere stimuleringsintensiteter end tykke fibre, mens et lille anode areal og en kort afstand mellem anode og katode øgede forskellen mellem den nødvendige intensitet for aktivering af tynde og tykke fibre, ved at begrænse strømspredningen i huden. En lille elektrode vil dog, som nævnt kunne

tilvejebringe praktiske problemer i forbindelse med korrekt elektrodeplacering. Denne praktiske begrænsning kan dog imødekommes ved at introducere flere anode-katode par og dermed øge sandsynligheden for at placere elektroden i nærheden af en nerve fiber terminal. Fra optimeringsresultaterne blev en ny elektrode designet, og i det tredje studie blev dette nye design testet gennem optagelser af evokerede potentialer og psykofysiske reaktioner. Det nye elektrode design blev sammenlignet med en konventionel patch-elektrode, som anvendt ved nerveledningsundersøgelser.

De evokerede potentialer viste forskellige mønstre og latenstider for den nye elektrode og patch elektroden. Disse forskelle skyldes formentlig en forskel i, hvilke nervefiberpopulationer de to elektroder aktiverer. Forskellene i de evokerede potentialer blev imidlertid ikke kvantificeret statistisk. Det kan derfor ikke udelukkes, at en vis mængde tykke nervefibre bliver aktiveret under stimulation med den nyudviklede elektrode. Ikke desto mindre vurderede forsøgspersonerne, at intensiteten af stimuli var højere, og at stimuli følte skarper for det nye elektrodedesign end patch-elektroden. Dette kombineret med en lavere sensorisk tærskel og længere reaktionstider, tyder på præferentiel aktivering af tynde nervefibre. Skarpheden og intensiteten af stimulationen steg med intensiteten af stimuli, hvilket kan antyde, at elektroden primært aktiverer tynde nervefibre, selv ved høje intensiteter.

I løbet af dette Ph.d.-arbejde blev en systematisk tilgang til elektrodedesign og udvikling, der udnytter fordelene ved modellering, introduceret. En ny overfladeelektrode til engangsbrug blev foreslået som et yderligere skridt mod et lovende værktøj til vurdering af beskadigelse af tynde sensoriske nervefibre.

# ACKNOWLEDGEMENTS

Firstly, I would like to thank my Ph.D. supervisor, associate professor Carsten Dahl Mørch, who gave me the opportunity to go on this Ph.D. adventure by encouraging me to apply for a Ph.D. fellowship at CNAP. He has been a great support throughout the entire journey, and I have a lot to thank him for. I would especially like to thank him for providing an open and trusting work environment that has allowed me to develop on both an academic and personal level. A special thanks also to professor Ole Kæseler Andersen for his feedback and knowledgeable insights and comments on scientific topics as well as academic life. Furthermore, I would like to express my sincere gratitude to assistant professor Jenny Tigerholm for everything she has done for me along the way, for always being ready to help with and discuss difficult topics, and for boosting my confidence by always including me and letting me know that my contributions and thoughts were valuable.

I would also like to thank professor Jan Buitenweg and Boudewijn van den Berg, from Twente University, for an interesting and valuable collaboration that unfortunately was limited to online meetings due to the COVID-19 pandemic. Despite this challenge, the collaboration went smoothly, and their great insights and helpfulness significantly increased the quality of the third study.

A great thanks to all of my excellent and wonderful colleagues at HST, CNAP, and the integrative neuroscience group. A special thanks to Kasper Leerskov for all the constructive hallway discussions and much-needed 'coffee' runs.

Finally, I would like to thank my friends and family for all their support along the way. A very special and heartfelt thanks to my boyfriend, Simon, who has been my rock throughout this Ph.D. journey, ensuring my mental stability, always knowing how to make me laugh, relax and helped me let go of my troubles when they weighed me down. I cannot thank him enough for the way that he has patiently handled my somewhat fluctuating mood, especially in the final phase of writing the thesis.





# TABLE OF CONTENTS

<b>Chapter 1. Introduction</b> .....	<b>13</b>
1.1. Preferential electrical stimulation of small fibers by specialized electrodes..	14
1.2. Models of electrical stimulation.....	15
1.3. Aim of the Ph.D. project.....	16
<b>Chapter 2. Electrical stimulation of peripheral nerves</b> .....	<b>19</b>
2.1. The skin and innervating nerve fibers .....	19
2.1.1. Epidermis .....	20
2.1.2. Dermis.....	20
2.1.3. Hypodermis .....	21
2.1.4. Nerve innervation of the skin.....	21
2.2. Electrical Properties of skin tissues.....	22
2.3. Electrical activation of neuronal tissue.....	25
2.3.1. The strength-duration relationship .....	26
<b>Chapter 3. Electrical stimulation of Peripheral nerves</b> .....	<b>29</b>
3.1. Volume conduction model of the skin.....	29
3.1.1. Model implementation of the skin.....	31
3.1.2. Model implementation of electrodes .....	33
3.1.3. Model implementation of the Electrode-skin interface .....	34
3.1.4. Boundary conditions.....	36
3.1.5. Meshing.....	37
3.2. Nerve fiber excitation model .....	38
3.2.1. Morphology.....	39
3.2.2. Voltage-gated ion channel dynamics.....	41
3.3. Model simulations .....	43
3.3.1. Electrode impedances .....	43
3.3.2. Time dependency.....	43
3.3.3. Area of selectivity.....	44
3.3.4. Strength-duration curve .....	46
3.3.5. Globalized Bounded Nelder-Mead optimization .....	46

3.4. Model sensitivity .....	50
3.4.1. Skin Thickness .....	50
3.4.2. Skin layer conductivity .....	51
3.4.3. Skin layer permittivity .....	51
3.4.4. Nerve fiber location .....	52
3.5. Model limitations .....	53
3.5.1. Simplifications and limitation of the volume conduction model .....	53
3.5.2. Simplifications and limitations of the nerve fiber model .....	54
3.6. Model validation .....	54
3.6.1. Impedance .....	54
3.6.2. Nerve fiber excitability .....	55
3.6.3. Skin thickness.....	57
<b>Chapter 4. A novel electrode design .....</b>	<b>59</b>
4.1. Optimized electrode dimensions .....	59
4.2. Novel planar concentric array electrode design .....	62
4.3. Performance of the novel planar concentric array electrode .....	66
4.3.1. Evoked potentials .....	66
4.3.2. PsychoPhysics .....	68
4.3.3. Comparison of the novel planar concentric array electrode with other existing electrodes.....	69
<b>Chapter 5. Conclusions and future perspectives.....</b>	<b>73</b>
5.1. Conclusion .....	73
5.2. Future perspectives.....	74
<b>Literature list .....</b>	<b>76</b>

# CHAPTER 1. INTRODUCTION

Small fiber neuropathy is defined as damage, degeneration, or sodium channel deficits of small diameter peripheral nerve fibers and has over the recent years become a well-recognized and continuously increasing healthcare problem. The minimum prevalence of small fiber neuropathy is 52.95 per 100,000 inhabitants and is expected to increase in the following years [1]. The cause and clinical presentation of the pathology vary greatly among patients making small fiber neuropathy difficult to both diagnose and treat. Treatment options for especially neuropathic pain patients are often insufficient, as only half of the subjects are approximated to achieve 50 % pain relief [2]. Additionally, the patients may have to try several different medications before reaching a helpful therapy. The quality of life for these patients is severely impaired [3], [4], and there is a current need for better clinically available tools to identify small fiber neuropathy and to develop personalized treatments for better patient outcomes. Electrical stimulation has been widely used for rehabilitation purposes[5], [6], pain relief [7], and the assessment of nervous system dysfunction in a variety of neuropathic pathologies [8]–[11]. Electrical stimulation introduces an electrical potential in the extracellular space resulting in a direct depolarization of the nerve fiber membrane, thus bypassing the sensory receptors and providing an artificial activation of the nerve. In clinical neurophysiology, the integrity and functional status of the peripheral nervous system are assessed through nerve conduction studies. It is a method proven to be a valuable tool for the assessment of pathologies with large fiber involvement as it may enable the localization of lesions and accurately characterize peripheral large fiber function [12]. However, this method cannot detect small fiber deficits, and in patients with pure small fiber neuropathy, the nerve conduction study will present with normal responses. For conventional electrical stimulation, the distribution of currents and the excitability properties of neurons causes large A $\beta$ -fibers to be recruited at a lower stimulation threshold than small A $\delta$ - and C-fibers. Consequently, any attempt to activate small fibers would always display concomitant activation of large fibers. Nevertheless, electrical stimulation has several advantages over other methods for the examination of peripheral nerve function, as it is cheap, easy to control, and has a high-temporal resolution with a direct influence on voltage-gated ion channels. Therefore, recent research has focused on reversing the nerve fiber recruitment order for electrical stimulation by the use of specialized electrodes.

## 1.1. PREFERENTIAL ELECTRICAL STIMULATION OF SMALL FIBERS BY SPECIALIZED ELECTRODES

To enable the use of electrical stimulation in the assessment of small peripheral nerve fiber function in neuropathic patients, specialized electrodes are necessary. Bromm and Meier [13] introduced an intra-cutaneous stimulation that elicited pricking sensations at the perception threshold level, suggesting preferential small fiber activation. Over the recent years, several electrodes with the purpose of activating small nociceptive fibers have been developed [14]–[19]. The electrodes differ in design and size. However, they are all designed to produce a high current density in the superficial skin layers and thereby activate small epidermal nerve fibers at a lower threshold compared to large fibers [15], [20], [21] that terminate within the deeper dermal skin layer [22], [23]. Such high current density distributions in the epidermis may be achieved with small area cathodes [20], [21], [24], while a concentric anode design may be introduced to limit the current spread to the dermal skin layer [15], [21], [24]. The specialized electrodes present lower perception thresholds than standard large area electrodes [15], [25], [26] and elicit sharp pinprick [14]–[17], [25] and burning [27], [28] sensations, indicating A $\delta$ - and C-fiber activation. Additionally, delayed reaction times [29] and cortical potentials [14], [29]–[31] of bilateral origin [25], [32] have been demonstrated. The cortical potentials elicited have likewise been shown to greatly diminish or completely abolish after application of local anesthetics [15], [28], [31], [33] or after small fiber denervation by prolonged application of capsaicin [29].

The possible diagnostic value of the specialized electrodes for small fiber neuropathy has been tested in a few pathologies and diseases such as; neuropathic pain [34], diabetes [11], [35], [36], hepatitis-C [37], and HIV [10], [38]. Pain thresholds have been suggested to be a reliable method to detect early changes in small fiber function in diabetic patients, as the pain threshold was increased in patients compared to controls [11], [36] and the threshold correlated with the progression of neuropathy [36]. Additionally, pain-related evoked potentials (PREP) with specialized electrodes for small fiber activation have been shown to be abnormal in HIV and diabetes-related neuropathies [34], [38]. PREPs have furthermore been suggested to be a potential method for following disease progression and patient outcomes, as the PREP alterations increased with the duration of disease [10], [34]. PREP latencies and amplitudes have also been found to correlate with the density of intra-epidermal nerve fibers (IENFD) [38]. These results are promising. However, the electrodes still lack stable stimulation and specificity of small fibers [36], [39]–[41]. The specialized electrodes elicit persistent and reproducible pinprick sensations. Nevertheless, the reproducibility of the perception threshold is only moderate compared to standard electrical stimulation [16], [42]. The planar electrode design introduced by Kaube et

al. [15] is likely the most debated electrode since the evidence for preferential small fiber activation is conflicting. Observations of evoked potential latencies have indicated conduction velocities in both the A $\delta$ -fiber [30], [31] and A $\beta$ -fiber range [39], [40]. La Cesa et al. [41] furthermore found that pinprick sensations were abolished after capsaicin-mediated nerve denervation. However, the evoked potentials were unaffected, even at low stimulation intensities. Similarly, for the intra-epidermal electrode design [14] and the micropatterned interdigitated electrode design [17], high stimulation intensities cause substantial co-activation of A $\beta$ -fibers [29], [43].

The existing electrodes have been empirically designed, and the electrode designs and the possible range of dimensions have not been fully explored in relation to small fiber activation. This may suggest a potential for improvement. To both simplify and systematize the process of analyzing the relatively large solutions space for the combination of electrode features and designs, computational modeling may be utilized. Computational models enable the search of large solution spaces and can be used to investigate specific hypotheses and improve the understanding of underlying processes of tissue excitation without the need for erroneous laboratory work.

## 1.2. MODELS OF ELECTRICAL STIMULATION

Computational modeling has been utilized to describe and better understand the effect an electrical field has on neural tissues and as a tool for designing stimulation of specific nerve fiber activation patterns[44]–[47]. The typical workflow for modeling electrical stimulation is a two-step hybrid approach combining a volume conduction model of the electrode and surrounding tissues with a nerve fiber excitation model. The volume conduction model simulates the current spread, and the electrical field produced by the electrode. This estimate of the electrical potential in the tissue is then introduced as the extracellular potential in a nerve fiber model that simulates the resulting changes in the transmembrane potential and the nerve fiber activity. This type of model has many application possibilities and has been used to study a broad spectrum of electrical stimulation for peripheral and central nerves and different electrical currents (anodic and cathodic) and pulses. To estimate the current distribution in the volume conduction part of the model, both analytical methods [48], [49], finite difference methods [50], [51], and finite element methods have been applied [20], [52], [53]. Analytical methods provide an exact general solution, picturing the overall effect of various parameters. Achieving the same overview of parameter effects when performing numerical analyses often comes with the expense of a great number of computations. However, analytical models are not applicable for more complex electrode and tissue geometries or when inhomogeneities in material properties exist [54]–[56]. For the second part, the nerve fiber model, the most often used approach is cable models of varying complexity. Model complexity concerns both the morphology and the inclusion of passive and active membrane components.

Often the morphology is simplified to a straight unbranched cable [49], [57]. However, most nerve fibers and particularly the nerve fibers innervating the skin, display substantial branching [22], [23]. For more complex models that include a branching structure in addition to active membrane components, multi-compartmental cable models are often used [58]. The multi-compartment cable model handles the branching of nerves and the variations in fiber diameter by dividing the nerve fiber into compartments that are small enough for the properties of interest to be uniform throughout the entire compartment. This discretization yields replacement of the continuous cable equation with a system of ordinary differential equations for the membrane potential [59].

Several models with a two-step hybrid approach have been proposed to describe transcutaneous electrical stimulation. However, only a few models have investigated electrode design in relation to small fiber activation. Mørch et al. [20] showed that a small area cathode is necessary to produce a high current density in the epidermis. Motogi et al. [51] investigated the needle length of an intra-epidermal electrode design and concluded that the highest *in situ* electrical field was produced when the needle was only just long enough to penetrate the outer stratum corneum. They, additionally, found that the anode-cathode distance did not affect the electrical field produced in the skin. This may suggest that cathode dimensions are the most important for achieving small fiber stimulation. However, the solution space investigated was relatively small in the two studies, and the anode characteristics and influence on small-fiber preferentiality have not been fully explored.

### 1.3. AIM OF THE PH.D. PROJECT

The Ph.D. project aimed to utilize computational modeling in the understanding of the effect electrode design has on current distribution and nerve fiber activation and to design a new electrode with the possibility to overcome the present limitations of electrical activation of the nociceptive system. This was achieved by subdividing the project into three main steps:

1. Develop and validate a computational model of the skin and innervating nerve fibers to compare existing electrodes for small fiber activation.
2. Utilize the model to investigate the influence of electrode parameters and to optimize the electrode design.
3. Design and evaluate the performance of a novel electrode design based on the results of the optimization in step 2.

To this end, the thesis is based on two peer-reviewed papers and a single paper submitted for review:

**Study I** [21]: Poulsen, A. H., Tigerholm, J., Meijs, S., Andersen, O. K., and Mørch, C. D., 2020, Comparison of existing electrode designs for preferential activation of cutaneous nociceptors, *J. Neural Eng.*

**Study II** [24]: Poulsen, A. H., Tigerholm, J., Andersen, O. K., and Mørch, C. D., 2020, Increased preferential activation of small cutaneous nerve fibers by optimization of electrode design parameters, *J. Neural Eng.*

**Study III**: Poulsen, A. H., Van den Berg B., Arguissain, F. G., Tigerholm, J., Andersen O. K., Buitenweg, J. R., Mørch C. D., XX, Novel electrode design for preferential activation of cutaneous nociceptors, submitted, *J. Neural Eng.*

In the following, these papers will be referred to as studies I to III. The outline for the dissertation is presented in Figure 1.1 and will more or less follow the chronological order of the project steps.

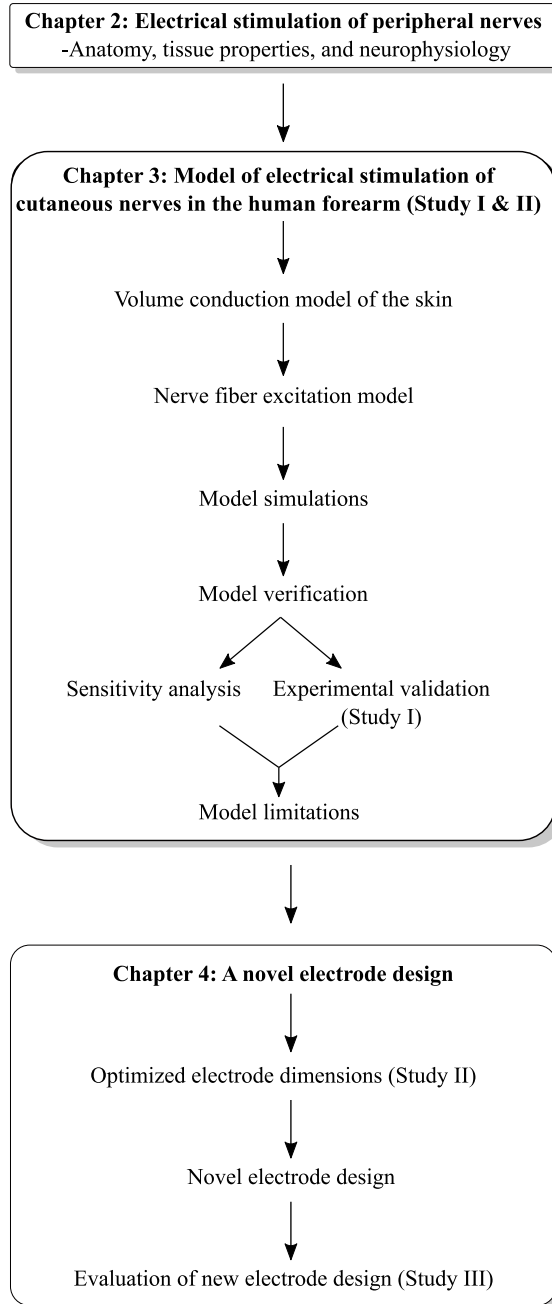


Figure 1.1: Outline of the Ph.D. dissertation.



# CHAPTER 2. ELECTRICAL STIMULATION OF PERIPHERAL NERVES

## 2.1. THE SKIN AND INNERVATING NERVE FIBERS

The skin acts as the first line of defense against external threats, protecting the underlying tissues and organs. In addition to its barrier function, the skin is an important sensory organ innervated by sensory nerve fibers that mediate information of temperature, touch, pressure, and pain, etc., and plays a major role in keeping homeostasis, regulating, for example, the blood pressure and body temperature [60]. The skin is a multilayered structure and is composed of three main layers; the epidermis, dermis, and the subcutaneous tissue, also known as the hypodermis (see skin structure in Figure 2.1) [60]. The population of neurons innervating the skin is heterogeneous as they express different specialized transducers for specific sensory functions. Additionally, the fiber distribution and density vary with different body regions and skin layers [61]–[63]. The nerve fibers of the skin are unipolar neurons that display only a single process emerging from the cell body. The nerve fiber axon projects from the periphery to the cell body, which is located in the dorsal root ganglia. From here, the nerve fiber axon enters the spinal cord and synapses with a second-order interneuron. The interneuron ascends to the thalamus after crossing to the opposite side of the spinal cord. In the thalamus, the interneurons synapse with third-order neurons, transmitting the signal to the sensory cortex. The functional interactions between the thalamus and the cortex lead to stimulus perception. While the activated neurons determine the sensation, the activated area in the somatosensory cortex enables the localization of the stimulus.

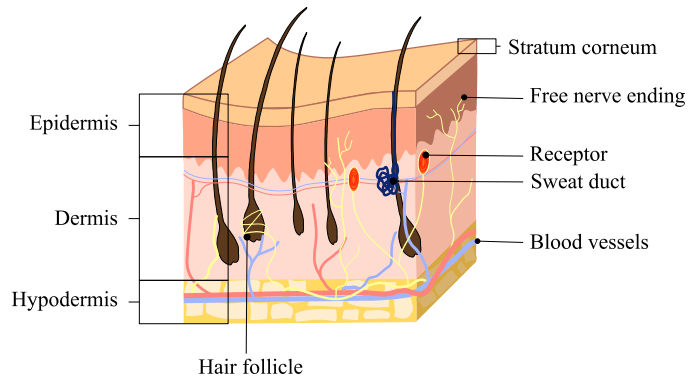


Figure 2.1: Anatomy and structure of the skin.

### 2.1.1. EPIDERMIS

The epidermis is the main barrier of the skin and is in a constant state of renewal. Cells in the basal epidermis undergo division and replace the more superficial keratinocytes of the skin surface. The epidermis is an avascular structure and depends on the diffusion of nutrients from the underlying vascular plexus in the dermis [60], [64]. Consequently, as the cells move towards the surface, their access to nutrients is reduced, and they lose viability. The viable epidermis can be subdivided into four layers; The stratum spinosum, stratum granulosum, stratum lucidum, and the stratum corneum, characterized by the state of the skin cells as they gradually lose viability with increased distance to the basal layer [60]. The first three layers have similar electrical and mechanical properties and are often referred to as the viable epidermis, while the stratum corneum properties greatly differ from the viable tissue as the stratum corneum is made up of dead keratinocytes that construct an efficient barrier from the external environment [60], [65]. The thickness of the epidermis varies with body site [66] and is the thickest in glabrous skin [67]. At the forearm, the viable epidermis has been reported to range from 56.6 to 100  $\mu\text{m}$  [66], [68]–[70]. The thickness of the stratum corneum layer ranges from 11.27 to 29  $\mu\text{m}$  [66]–[68], [71], at the site of the forearm.

### 2.1.2. DERMIS

The dermis is the main contributor to the skin's mechanical properties and consists primarily of collagen and elastin fibers [64]. The dermis is connected to the epidermis by a papillary interface that provides a high contact surface area and thereby increases

the exchange of nutrients between the epidermis and dermis [60], [65]. Apart from a rich network of capillaries in the superficial dermis, the dermis also contains sensory receptors and nerve endings, hair follicles, sebaceous glands, and sweat gland, some of which penetrates all the way through the epidermis to the skin surface [60], [65]. The thickness of the dermal skin layer is like the epidermis, dependent on the body site, and varies between 1-2 mm [72], [73].

### **2.1.3. HYPODERMIS**

The hypodermis is mainly composed of collagen and adipocytes. Due to the high content of fat, the hypodermis protects against physical shock and functions as a heat generator and insulator [64], [65]. Additionally, the hypodermis functions as an energy storage. Blood vessels and nerves that supply the epidermis and dermis connect via the hypodermis. The thickness of the hypodermis varies greatly within and between individuals [64].

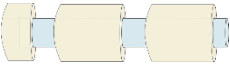

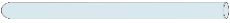
### **2.1.4. NERVE INNERVATION OF THE SKIN**

Generally, three types of nerve fibers innervate the skin (see Table 2.1). Small-diameter nociceptors may be classified into thinly myelinated A $\delta$ -fibers and unmyelinated C-fibers based on their diameter, structure, and conduction velocity. These fibers innervate the epidermal skin layer. They arise from the subepidermal neural plexus, from which they ascend vertically in an irregular winding path between the keratinocytes of the epidermis, and in general, terminate as free nerve endings in the stratum spinosum or stratum granulosum [23]. Any myelination is lost as the axons pass the dermal-epidermal junction, making the nerve fibers indistinguishable within the epidermal skin layer [22], [23]. Within the epidermis, branching of the axons may occur up to several times [74]. A $\delta$ -fibers are approximately 1-6  $\mu$ m in diameter and have conduction velocities of 5-30 m/s [75]. These fibers mainly mediate information of noxious mechanical stimulation, however, some are also activated by high-intensity temperature stimuli [76]. The unmyelinated C-fibers constitute approximately 70 % of all cutaneous nerve fibers and are thereby the most abundant [77]. C-fibers are slowly conducting fibers (0.4-2.0 m/s) with diameters of 0.2-1.5  $\mu$ m [75]. C-fibers have been described to mediate nociceptive information of noxious chemical, thermal, low threshold mechanical stimuli, and itch [76].

Large myelinated non-nociceptive, A $\beta$ -fibers, provide a rich innervation of specialized mechanoreceptors, vascular structures, and hair follicles in the deeper dermis. In hairy skin, the A $\beta$ -fibers are most abundant around hair follicles, and only a few fibers are present in the superficial part of the dermis [22]. A $\beta$ -fibers have a

diameter of 6  $\mu\text{m}$  or more and are fast conducting fibers with conduction velocities up to 100 m/s [77]. These fibers are mechanosensitive fibers and respond to non-noxious touch, pressure, and vibration.

Table 2.1: Properties of different sensory nerve fibers [75].

Fiber type	Diameter	Conduction velocity	Termination within the skin	Mediated sensations
A $\beta$ -fiber 	>6 $\mu\text{m}$	36-100 m/s	Dermis	Touch, vibration
A $\delta$ -fiber 	1-6 $\mu\text{m}$	5-30 m/s	Epidermis	Pain and temperature
C-fiber 	0.2-1.5 $\mu\text{m}$	0.4-2 m/s	Epidermis	Pain, temperature, and itch

## 2.2. ELECTRICAL PROPERTIES OF SKIN TISSUES

All biological tissues display dielectric characteristics and may be electrically characterized in terms of their ability to polarize and conduct current. The polarizability of a material is described by its permittivity. For biological tissues, the permittivity typically displays three major frequency regions, for which the permittivity decreases as a function of increasing frequency. These regions are often referred to as the  $\alpha$ -,  $\beta$ -, and  $\gamma$ -dispersion and may be coupled to specific electrochemical mechanisms [78] (see figure Figure 2.2). The  $\alpha$ -dispersion is generally believed to be associated with the polarization of ions at or near the boundary of the cell membrane [79], [80] and occurs in the low-frequency region. The  $\beta$ -dispersion ranges from a few kHz to hundreds of MHz and is generally related to structural changes and charging of the cell membrane. In the frequency range from

MHz to GHz, the  $\gamma$ -dispersion is dominant and is mainly an attribute of the relaxation of water, ions, and small molecules in the intracellular fluid, and is thus highly dependent on the water content of the tissue [79]. The conductivity of biological tissues likewise varies with frequency but in the opposite direction, with increasing conductivity for higher frequencies [81], [82]. The slope of the frequency-dependent changes in conductivity is additionally much smaller than for the permittivity [82], and in the low-frequency range, conductivity is often assumed to be constant, as the frequency-dependent changes are rather small [83].

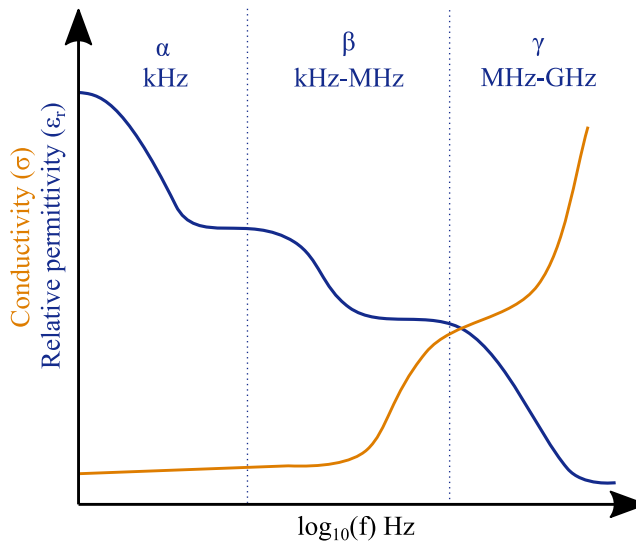
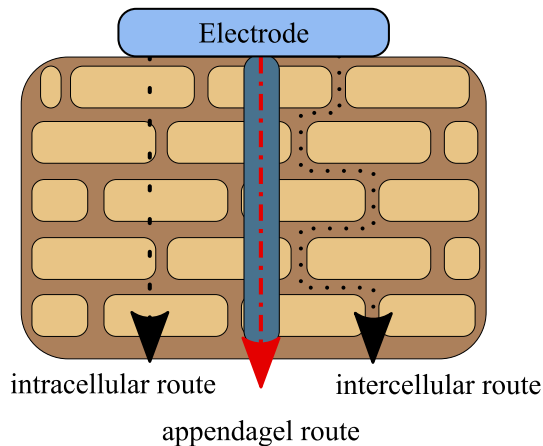


Figure 2.2: General schematic of the frequency dependencies of the permittivity and conductivity of living tissues.

The electrical properties of the skin do not only vary with frequency but also the applied current and temperature have an effect [79], [84]. An increase in temperature produces an increase the conductivity, especially in the low-frequency range. Consequently, as the temperature is increased, the conductivities at low frequencies approach the conductivity at high frequencies, and they become almost identical when the temperature rise starts to cause irreversible membrane damage [85]. An electric current flow through the skin increases conductivity, likely due to changes in membrane permeability. The conductivity dependency on current flow is larger in hairy compared to glabrous skin [84].

Generally, an applied current to the surface of the skin may take three different paths. At low frequencies, the current will mainly follow the extracellular path, but at higher frequencies, the membranes of the cell are electrically shorted, allowing current to flow through the cell. The third path is through skin appendages such as sweat ducts and hair follicles, through which the current will mainly flow when the pores are active, and the water content is high (see current pathways in Figure 2.3).



*Figure 2.3: The routes of the current through the skin tissues. At low frequencies, the cell conducts poorly compared to the extracellular electrolyte and thus limits the current flow to the extracellular fluid. For higher frequencies around and above the frequency range of the  $\beta$ -dispersion, the cell membrane barrier breaks down, allowing the current to flow through the cells. The last route the current may take is through skin appendages, such as sweat ducts, that, when filled, provide a low impedance pathway for the current.*

The literature exhibits considerable differences in the electrical properties of the skin, likely, due to differences in methodology, as the methods used for both tissue preparation and estimation of conductivities and permittivities may greatly affect the outcome [86]. Additionally, the electrical properties of the skin are often measured for whole skin samples. However, the properties of the different skin layers are very different as the cell composition and the water content varies greatly with the distance to the skin surface. Whole skin samples are believed to mainly reflect stratum corneum properties, as this skin layer is very different from the underlying tissue and is the most resistive skin layer with impedances up to approximately  $5\text{ M}\Omega$  [87]. Yamamoto and Yamamoto [88] investigated the impedance of the skin by tape stripping and found the impedance of the outer keratin layers to be much higher than the impedance of the viable skin layers exposed after stripping. These differences between the stratum corneum and the viable skin layers were most evident in the low-frequency range, and in general, the stratum corneum is considered to dominate skin impedance

up to around 1 kHz [89]. The conductivity of the stratum corneum is much lower than for the remaining epidermis, and permittivity values are likewise lower for the stratum corneum [88]. The values vary with skin condition and may change significantly as a function of water content. This is specifically reflected in the difference between wet and dry skin presented by Gabriel et al. [90]. The viable epidermis and dermis are often considered to be homogeneous and isotropic tissue layers with similar properties. However, Tavernier et al. [91] showed an anisotropic nature for the electrical properties, with slightly different permittivity and conductivities in the horizontal and vertical direction. Furthermore, the dermis displayed higher conductivity and permittivity compared to the epidermis. The hypodermis mainly consists of lipids, and the water content is relatively sparse, which is likely the reason for this skin layer's low conductivity compared to the viable epidermis and the dermis [92], [93].

### **2.3. ELECTRICAL ACTIVATION OF NEURONAL TISSUE**

The ionic composition of the extracellular fluid surrounding a neuron and the intracellular fluid of the neuron greatly differ and gives rise to a resting membrane potential of approximately  $-70\text{mV}$ . Excitation of the neuron occurs when the membrane is depolarized, but to generate an action potential and transmit information from the periphery to the central nervous system the depolarization must be large enough to reach a threshold level of the transmembrane potential of approximately  $-55\text{mV}$  [94]. At this level of depolarization, the voltage-gated sodium channels in the membrane open, and sodium flows into the cell, resulting in a rapid increase in the membrane potential [94]. As the transmembrane potential approaches  $+30\text{mV}$ , the sodium channels are inactivated, and voltage-gated potassium channels open, and potassium ions move from the inside of the cell to the outside, and repolarization of the membrane is initiated [94]. When the membrane potential reaches the resting potential, potassium channels start to close. However, until all channels are closed, ions continue to flow, and a brief hyperpolarization occurs before the membrane potential returns to the resting state [94]. An action potential propagates along the entire membrane until it reaches the synaptic terminals. Propagation speed and nerve fiber excitability are highly related to the diameter and myelination of the axon [75], [94].

Nervous tissue may be artificially activated by the application of external currents through surface electrodes. Applying a current to the cathode will initiate the build-up of negative charges at the electrode, causing ions in the tissue to move. The resulting potential difference due to ion movement in the extracellular space may generate an action potential in nerve fibers located in the stimulated tissue, as the

extracellular space becomes more negative and the membrane is depolarized [95]. Within the extracellular space under the anode, accumulation of positive charges occurs, and the nerve fiber displays regions of hyperpolarization (see Figure 2.4).

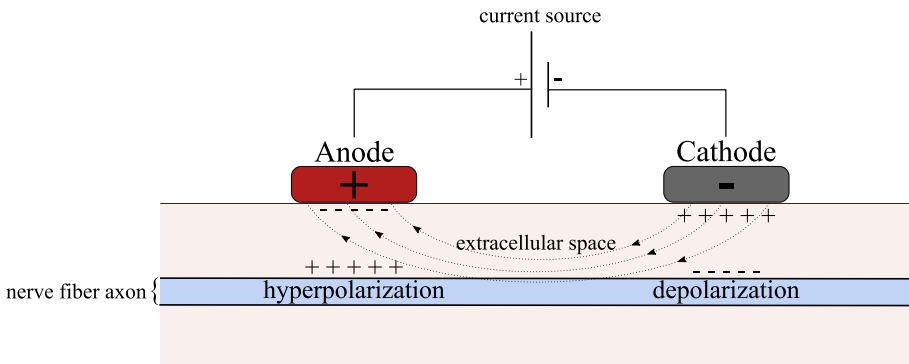


Figure 2.4: Illustration of electrical surface stimulation of a peripheral nerve fiber axon.

An action potential is generated when the membrane depolarization reaches a threshold limit. From the generation site, the action potential propagates along the axon by the spread of local currents that depolarize adjacent proportions of the nerve fiber membrane [94]. For unmyelinated nerve fibers, a continuous propagation occurs, whereas myelinated fibers only respond to depolarization at the nodes of Ranvier and thereby ‘jumps’ over intermodal segments, allowing faster propagation of the action potential [94]. The activation threshold of a nerve fiber may be defined as the minimum current amplitude required to generate a propagating action potential. Large non-nociceptive sensory fibers ( $A\beta$ -fibers) are more excitable than small nociceptive fibers ( $A\delta$ - and C-fibers) due to both fiber diameter and myelination. Consequently, large fibers display a lower activation threshold than small fibers when applying conventional electrical surface stimulation. The activation threshold of a neuron at a specific distance from the stimulation electrode exhibits a strength-duration relationship with the width of the stimulation pulse [96], [97]. For short pulses, higher intensities are needed compared to longer stimulation pulses.

### 2.3.1. THE STRENGTH-DURATION RELATIONSHIP

The required current to activate a nerve fiber decrease with increasing duration of the stimulation pulse [97]. This is known as the strength-duration relationship. The



strength-duration relationship may convey information about nerve fiber excitability and the membrane properties of the neuron and differs between different nerve fiber types [42], [97], [98]. The strength-duration relationship is mainly described by the rheobase and the chronaxie. The rheobase is the current amplitude needed to reach the activation threshold to an infinitely long stimulation pulse, while the chronaxie, also known as the time constant, is defined as the duration for which the current to reach the activation threshold is two times the rheobase [97].



# CHAPTER 3. ELECTRICAL STIMULATION OF PERIPHERAL NERVES

Models of electrical stimulation may provide great insights into the behaviors of biological tissues and the mechanism involved in observed experimental phenomena. As the modeling approach allows searches of large parameter spaces, models may also enable predictions of experimental outcomes and may be utilized as assistive tools to design new experiments and protocols. In this project, modeling was used as a tool to investigate how different electrode designs and specific design parameters affected the recruitment order of peripheral nerve fibers in the skin, and thereby tune the electrode design and dimensions to preferentially activate small nociceptive nerve fibers.

The model was implemented in a widely used approach that may be referred to as both two-step and hybrid modeling. Firstly, the potential distribution produced by the electrode was described by the use of a volume conduction model of relevant tissues and electrode designs, and secondly, two nerve fiber models were used to describe the behavioral response of the nerve fibers to the applied electrical stimulation.

## 3.1. VOLUME CONDUCTION MODEL OF THE SKIN

The current and electrical potential distribution produced in the skin by an external electrical stimulation may be modeled by a geometrical representation of the tissue and its electrical properties and is explained by Maxwell's equations. Often the inductive effects and the wave propagation can be assumed negligible, as the changes within the distribution of the electrical potential are slow. Thereby, the electro-quasistatic approximation of Maxwell's equations, neglecting the magnetic induction, can be used (see equations (3.1), (3.2), (3.3), and (3.4)).

$$\nabla \times \mathbf{H} = \mathbf{J} + \frac{\partial \mathbf{D}}{\partial t} \quad (3.1)$$

$$\nabla \times \mathbf{E} = 0 \quad (3.2)$$

$$\nabla \cdot \mathbf{B} = 0 \quad (3.3)$$

$$\nabla \cdot \mathbf{D} = \rho \quad (3.4)$$

Where  $\mathbf{E}$  and  $\mathbf{B}$  denote the electric and magnetic fields, respectively.  $\mathbf{H}$  denotes the magnetization,  $\mathbf{J}$  is the current density,  $\mathbf{D}$  is the dielectric displacement, and  $\rho$  is the volume charge density. In the quasistatic case, the electric and magnetic fields are considered to be distinct uncoupled phenomena, and the electric potential may be calculated based only on equations (3.2) and (3.4), which involve the electrical field. The expression in equation (3.2) disclose that the electrostatic field is curl-free and thus can be described by the gradient of the potential ( $V$ ) (see equation (3.5))

$$\mathbf{E} = -\nabla V \quad (3.5)$$

For homogeneous, linear, and isotropic materials, the dielectric displacement may be described by the permittivity ( $\epsilon$ ) of the material and the electric field, also known as the constitutive relation of the material (see equation (3.6))

$$\mathbf{D} = \epsilon \mathbf{E} \quad (3.6)$$

Utilizing Ohms law (see equation (3.7)) and the equation of continuity (see equation (3.8)), the differential equation that describes the electric potential within a volume conductor can be deduced (see equation (3.9)).

$$\mathbf{J} = \sigma \mathbf{E} \quad (3.7)$$

$$\nabla \cdot \mathbf{J} + \nabla \cdot \frac{\partial \mathbf{D}}{\partial t} = 0 \quad (3.8)$$

$$-\nabla \cdot (\sigma \nabla V) - \nabla \cdot \left( \epsilon \nabla \frac{\partial V}{\partial t} \right) = 0 \quad (3.9)$$

In steady-state, the time dependency is ignored, and equation (3.9) reduces to the Laplace formulation (see equation (3.10))

$$-\nabla \cdot (\sigma \nabla V) = 0 \quad (3.10)$$

The approach to solving the differential equations may be either analytical or numerical. The analytical approach is typically faster than the numerical approach, and closed-form solutions often exist. However, detailed, complex, and small geometries may not be solved analytically. Numerical methods such as the Finite Volume Method (FVM) and the Finite Element Method (FEM) are able to model very complex geometrical structures and also provide the possibility to locally refine the

meshing in certain areas with large and fast changes or in areas of particular interest. The FVM provides robust handling of both linear and non-linear cases and only needs the evaluation of the flux at the boundaries between model cells. However, the FEM is often considered a more powerful method as higher-order spatial discretization may be derived.

Current sources for electrical stimulation of nerve fibers in the skin may be implemented in several ways within a finite element model. Appropriate geometries, skin properties, and model boundary conditions are necessary to achieve accurate and reliable approximations of the potential distribution in the skin and, thereby, accurate nerve fiber activation thresholds.

### **3.1.1. MODEL IMPLEMENTATION OF THE SKIN**

The skin is a relatively complex structure that is constituted by a large variety of cell types and shapes. An extracellular fluid makes up the space between cells. Each type and shape of cells and the extracellular fluid has different electrical properties that may be modeled. However, simpler models of higher abstraction levels are often used, as the purpose of volume conductor models for modeling electrical stimulation is most often to capture the overall behavior of the skin tissue and not necessarily to account for individual cell type behaviors and their interaction. In many applications, the skin is modeled as a single combined entity. However, for the model in the present project, four distinct layers of the skin were implemented; the stratum corneum, the viable epidermis, the dermis, and the hypodermis. This more detailed layered structure was chosen due to the nerve fiber trajectories and termination depths within the skin. Both large and small fibers run through the hypodermis before they penetrate into more superficial skin layers where the large fibers terminate in the dermis, and the small fibers terminate in the epidermis. To take the possible effect of transition regions on nerve fiber activation into account and to describe the difference between the tissues of nerve fiber termination (dermis and epidermis), it was considered more accurate to include these layers as distinct layers within the model. Further division of the epidermis into the stratum corneum and the viable epidermis was done as the stratum corneum display very different electrical properties and is the main contributor to the skin's resistive nature. The effect of the stratum corneum was considered to be even more important as planar surface electrodes with small areas were investigated. The electrical properties implemented in the model are provided in Table 3.1 and were based on literature, including both studies of properties and previous skin models. The frequency dependencies of the stratum corneum, epidermis, and dermis were estimated by fitting graphical data from Yamamoto and Yamamoto [88] and Tavernier et al. [91]. The data were thus extracted from the figures within the papers, a procedure that has likely introduced some bias to the original data due to reading inaccuracies.

Table 3.1: Electrical properties of the implemented skin layers. The applied minimum and maximum values were used in the sensitivity analysis of the model [21], [24]. The model implemented values were used in the simulations investigating electrode designs in studies I and II.

Model structure	Property	Min	Model implementation	Max
<b>Stratum corneum</b>	Thickness ( $\mu\text{m}$ ) [66]–[69], [71], [99]	11.27	20	30
	Conductivity (S/m) [88]	0.00002	$\frac{1}{1.339 * 10^5 * f^{-0.1099} * (-3.65) * 10^4}$	0.002
	Relative permittivity [88]	1000	$1.44 * 10^4 * f^{-0.459} + 1,285$	3000
<b>Viable epidermis</b>	Thickness ( $\mu\text{m}$ ) [66], [68], [69]	56.6	82	100
	Horizontal Conductivity (S/m) [91]	0.58	0.95	1.32
	Vertical conductivity (S/m) [91]	0.13	0.15	0.17
	Horizontal relative permittivity [91]	6.65e3	$-1.332 * f^{-1.212} + 3.731 * 10^5$	4.07e5
	Vertical relative permittivity [91]	2.64e4	$6.32 * 10^6 * f^{-0.562} - 1.196 * 10^4$	1.04e5

<b>Dermis</b>	Thickness ( $\mu\text{m}$ ) [72], [73], [100]	838	1300	2000
	Horizontal conductivity (S/m) [91]	1.74	2.57	3.4
	Vertical conductivity (S/m) [91]	1.29	1.62	1.95
	Horizontal relative permittivity [91]	1.06e5	$5.394 * 10^8 * f^{-0.012} + 2.301 * 10^5$	1.82e6
	Vertical relative permittivity [91]	5.32e4	$3.255 * 10^9 * f^{-1.25} - 8,433$	5.37e5
<b>Hypodermis</b>	Thickness ( $\mu\text{m}$ ) [20], [52]	3,000	5000	6,000
	Conductivity (S/m) [92], [93], [101]	0.01	0.023	0.1
	Relative permittivity [92], [93], [101]	800	1000	150,220

---

### 3.1.2. MODEL IMPLEMENTATION OF ELECTRODES

Four existing electrodes for small fiber activation; intra-epidermal electrode [14], planar concentric electrode [15], pin electrode [18], planar array electrode [19], and

one regular patch electrode (Ambu® neuroline 700), known to preferentially activate large fibers, were implemented (illustrations of the electrode designs can be found in figure 1 of study I ). The intra-epidermal design consisted of a needle cathode and a concentric anode ( $0.28 \text{ mm}^2$ ). The planar concentric electrode had a similar design with a concentric anode ( $8.64 \text{ mm}^2$ ) around a planar small area cathode ( $0.5 \text{ mm}$  in diameter). The pin electrode consisted of 15 interconnected small area cathodes ( $0.2 \text{ mm}$  in diameter) placed in a circular pattern and with a larger concentric anode ( $876.5 \text{ mm}^2$ ) surrounding the cathodes. The planar array electrode had two rows of 6 square cathodes ( $0.6 \times 0.6 \text{ mm}$ ), all interconnected. A rectangular anode ( $5 \times 25 \text{ mm}$ ) was placed on each side of the cathode rows. The patch electrode configuration consisted of a rectangular cathode and anode ( $1.5 \times 2 \text{ cm}$ ), placed  $2 \text{ cm}$  apart. The small area electrodes for small fiber activation were made of metal alloys. Adding the material composition to the model would enable simulations of the current distribution across the electrode and incorporate small inhomogeneities within the metal that could potentially have an effect on the current densities within the skin and the resulting nerve fiber activation. Nevertheless, the electrode material was omitted because the great differences in electrical properties between the highly conductive electrode metals and the highly resistive stratum corneum posed critical convergence issues for the model, in addition to substantially increasing the computational time and load.

For the large area patch electrode, the hydrogel which is in contact with the skin was included. The hydrogel layer has an important effect on the current densities and current distribution in the skin. For high gel resistivity, the current distribution is more localized beneath the electrode, and the current distribution across the electrode is more uniform [102]. Hydrogels of high resistivity may thus decrease the influence of larger skin inhomogeneities but may also introduce inhomogeneities within the gel itself that may cause local areas of high current densities [103].

### **3.1.3. MODEL IMPLEMENTATION OF THE ELECTRODE-SKIN INTERFACE**

Having a closer look at the electrode-skin interface, transduction of charge carriers occurs from the electrons that carry charge in the electrode material and to the ions that carry charge within the tissue. The processes of charge transfer at the interface may be either non-Faradaic or Faradaic. For non-Faradaic reactions, no electrons are transferred across the electrode-skin interface, but sufficient charging of the interface courses ions in the tissue to move and generate currents. Hence, for non-Faradaic reactions, the interface may be modeled as a capacitor, within which charge may be



stored and recovered when a potential is applied to the electrodes [104]. Faradaic reactions occur when a charge is injected and electrons transferred between the electrode and the tissue through processes of reduction and oxidation on the electrode surface. The Faradaic reactions may either be reversible or irreversible. For reversible reactions, the chemical products do not diffuse far from the electrode surface, and thus reversing the direction of the current may also reverse the faradaic reactions. If the chemical products from the Faradaic processes diffuse too far away from the electrode interface, they become irreversible and may cause damage to the electrode and tissue.

The electrode-skin coupling has non-linear behaviors and can operate in a wide range of frequencies and current densities. The interface is an important part to include when trying to simulate electrical stimulation of tissue in a realistic manner. The interface may, in general, be modeled by a resistor and capacitor in parallel, with values of the resistance and capacitance that are dependent on the electrode material and geometry. The values of the resistance and capacitance of the interface both depend on the frequency and current density. The phase characteristics of the electrode-skin interface impedance are mainly affected by frequency, and the phase angle is relatively constant for low frequencies but decreases with increasing frequency in the higher frequency ranges [105]. The phase angle does not change much with the current density. However, the magnitude of the impedance is highly dependent on current densities. At low current densities, the values of the interface are relatively constant, however, for higher current densities, a rapid increase in the capacitance and decrease in the resistance can be observed with increasing current densities. This phenomenon occurs over a large frequency span but is most pronounced in the low-frequency range [105]. This behavior of the interface results in a decreased impedance of the electrode-skin interface with increasing current density, why the interface is more important when low current densities are involved. Hence, to explain the impedance of especially large area electrodes and the electrical stimulation in close proximity to the electrode, the inclusion of the interface within the model is crucial [106], [107].

The conductivity and relative permittivity of the interface was adopted from the resistances and capacitances for wet and dry electrodes presented by Chi et al. [108]. The small area electrodes were all dry electrodes, whereas the regular patch electrode was specified as wet due to the hydrogel layer. The hydrogel was added to the model of the patch, and the electrical properties of the hydrogel were equal to the ones implemented in the model by Mørch et al. [20]. Electrochemical effects of the interface were not implemented in the model as they tend to cause only minor negligible changes in the conductivity and permittivity of the interface when current regulated stimulation is used [109].

### 3.1.4. BOUNDARY CONDITIONS

Defining appropriate boundary conditions is essential to achieve a meaningful representation of a physiological system. The solution of the differential equations is uniquely defined by the boundary conditions, and thus the choice of boundary conditions has a great effect on the quality of the solution. It is, however, not always obvious how to best implement boundary conditions, and multiple implementations have been used for modeling electrical stimulation of tissues [20], [106], [109], [110]. Pelot et al. [110] investigated some of the common ways of modeling current sources for metal electrodes. They compared the accuracy and runtime and found the Neumann boundary condition of distributed current density at the electrode surface to be the most appropriate. However, it is important to notice that the Neumann conditions for current stimulation assume a homogeneous current distribution across the electrode surface, which is a simplification, as the current across an electrode is not likely to display a homogeneous distribution in practice [106]. Consequently, Joucla et al. [107] recommend the use of a Robin boundary condition to model electrical stimulation. The Robin boundary condition is a combination of the Neumann and Dirichlet boundary conditions defining the current flowing through a given point on the electrode as the product of the surface conductance and the potential drop over the interface. Thereby, a non-homogeneous current density across the electrode surface may be modeled. For small area electrodes, however, the current distribution across the electrode may be assumed to be more or less uniform, and the Neumann condition is then sufficient to model the electrode and the interface. Consequently, normal current density conditions were used to model the current stimulation in studies I and II. An inward current of 1mA was applied to the cathode, while an equal outward current (-1mA) was applied to the anode. For the intra-epidermal electrode design, which had a needle cathode, the current density may not be uniform to the same extent as the planar electrodes, as the current would tend to have higher concentrations at the pointy electrode tip. However, including a Robin boundary condition for this electrode did not alter the excitation of the nerve fiber models, and consequently, the Neumann condition, as recommended by Pelot et al. [110], was used for all electrodes. All implemented boundary conditions of the models used in studies I and II are illustrated in Figure 3.1. The bottom of the model was grounded using a Dirichlet boundary condition setting the potential to zero. This procedure superficially drags the potential to zero at the bottom of the model and may potentially impose a bias on the potential at the nerve fiber location. Increasing the hypodermal thickness likewise increases the distance from the electrodes to the ground and thereby decreases the potential influence of the boundary condition. The effect of the ground condition can thus be tested by increasing the hypodermal thickness and assess the degree of potential change at the nerve fiber location.

Increasing the thickness of the hypodermal skin layer beyond 5000  $\mu\text{m}$  did not alter the electrical potential at the nerve fiber locations to an extent that influenced the nerve fiber activation. Finally, conditions of current continuity was applied to all internal boundaries, while the remaining external boundaries were perfectly insulated. Thereby the current was restricted inside the model. To make sure the insulating boundaries did not affect the model solution a convergence study was conducted to determine the model size. The model size was increased in increments of 1 cm until the electrical potential changed by less than 0.1 mV between increments.

### Model boundary conditions

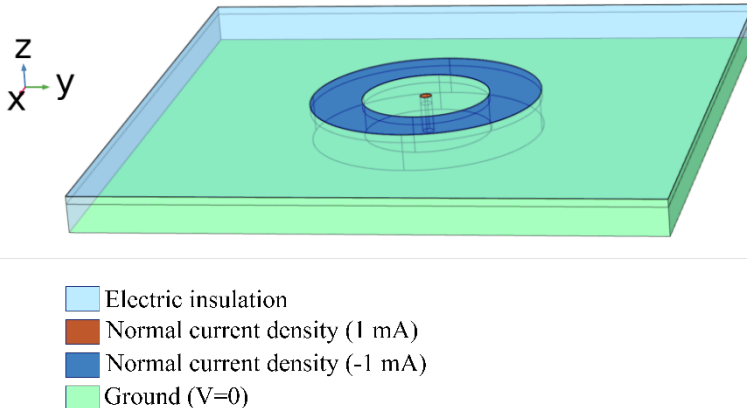


Figure 3.1: Implemented boundary conditions in the volume conduction model.

### 3.1.5. MESHING

The density and quality of the model mesh are essential to obtain accurate simulations of the electrical potential. The mesh should be fine, especially in the regions of interest, such as the nerve fiber locations, and in areas for which the potential is expected to display fast changes, as is the case at the electrode border. However, increasing the mesh density comes with a cost of computational effort and time, why a balancing between accuracy and time is often required. To ensure an acceptable balance, the mesh size was refined until the potential change over the entire nerve

fiber location was less than 0.1 mV. The criteria of 0.1 mV were applied as smaller changes would not affect the simulations of nerve fiber activation.

In order to decrease the risk of inverted or collapsed elements, and elements of a high aspect ratio, the growth rate was restricted to 10 %. Additionally, mesh quality was evaluated by the skewness measure. This measure punishes mesh elements that have angles deviating from that of an ideal element [111]. The mesh was refined until all elements displayed quality measures below an acceptable limit of 0.1.

### **3.2. NERVE FIBER EXCITATION MODEL**

The effect of the extracellular potential on a nerve fiber has been modeled with varying degrees of complexity. The simplest way to model this influence is by the second spatial derivative of the extracellular potential along the nerve fiber, also known as the activating function [49]. The activating function pinpoints locations of depolarization and hyperpolarization and does not require the implementation of nerve fiber properties. Consequently, the activating function may be used to determine the most likely sites of nerve fiber activation and propose an estimate of the relative efficiency of a certain electrode design. However, the function does not on its own enable estimation of the membrane potential and the nerve fiber response to a current source. Additionally, a simple model like the activating function cannot explain the differences in nerve fiber activation due to, for example, nerve fiber diameter or fiber type. Whereas the activating function provides a description of the source or driving factor of the membrane potential, a linear cable model may include specific nerve fiber properties that can describe the passive behaviors of the membrane. Only the capacitive membrane properties are included while the membrane conductance is kept constant. Such linear models are therefore also often referred to as passive models. No ion-channel dynamics are included in the passive model, and thus it may not explain the nerve fiber response or the generation of action potentials. Consequently, a specific degree of membrane depolarization is used as a threshold value above which fiber activation is assumed. Setting this threshold value is, however, not trivial as the threshold transmembrane voltage varies with pulse width [112] and stimulus location relative to the nerve fiber [113]. Active models that implement the dynamics of voltage-gated ion channels are thus preferred when an accurate estimate of the activation threshold is needed. The inclusion of the ion channel dynamics enables the modeling of the action potential generation and propagation and is thereby more comparable to neurophysiological properties, but also increase the computational load.

For studies I and II, an active model of a thinly myelinate A $\delta$ -fiber and a model of a large A $\beta$ -fiber presented by Tigerholm et al. [46] was implemented. These models were specifically designed to account for fiber type differences and had been shown to explain experimental data for the activation of large and small fibers [46], [47]. The A $\delta$ -fiber and A $\beta$ -fiber models were based upon a previously published C-fiber model [58], which in a recent comparison study was shown to best reproduce experimental data from C-fibers [114].

### 3.2.1. MORPHOLOGY

The morphology of the nerve fiber may have an impact on the nerve fiber activation and propagation properties. An abrupt bend in the nerve fiber trajectory may result in nerve fiber depolarization and excitation at the bend [115]. Additionally, the finer details of the myelin structure in the proximity of a node of ranvier and their associated electrical properties have been suggested to be important mechanisms involved in the action potential after potentials [116], [117]. As a consequence of these morphological influences, nerve fiber models tend to vary greatly in the complexity of the implemented morphological structures. The choice of morphology, as well as other modeling choices, depends mainly on the specific research question, and there will always be a tradeoff between the accuracy of the morphological representation and the model complexity.

For the small morphologies around the nodes of ranvier, the most detailed models include segments of the nodes themselves, the paranode, where the myelin attaches to the axonal membrane, the juxtaparanode region adjacent to the paranode, and the internodal regions accounting for approximately 99% of the total length of a myelinated nerve segment [118]. Such detailed models are referred to as double cable models as the myelin is modeled separately from the axon, and the resistive properties of the periaxonal space between the myelin and the axon is included [117]. The double cable model was introduced to enable modeling of the refractory period following an action potential and to investigate the underlying mechanisms. However, the double cable model is mostly applied with a straight axon process as branching structures are more difficult to implement and increase the computational load substantially [119]. In the present project, the general trajectory of the peripheral nerve fibers was considered of particular relevance when comparing small and large fiber activation. Consequently, a simpler single cable model providing adequate accuracy for activation threshold prediction was preferred. The model used in studies I and II was a single cable model including the general course of the nerve fiber within the skin together with the nodal, internodal and juxtaparanodal regions (see Figure 3.2).

### Morphology of the nerve fiber models

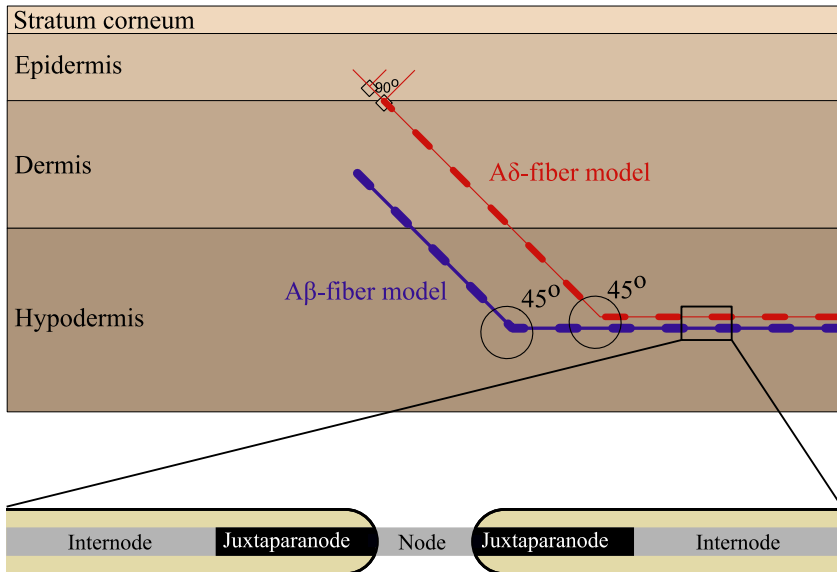


Figure 3.2: Illustration of the nerve fiber models implemented in studies I and II. The models ran horizontally within the hypodermis before making a 45-degree bend towards the skin surface. The Aβ-fiber model terminated within the dermis, while the Aδ-fiber model continued into the epidermis. The myelin of the Aδ-fiber model was lost as the fiber crossed the dermal-epidermal junction. Furthermore, the Aδ-fiber model displayed two secondary branches with a 90-degree angle from the main branch. The nerve fiber models were single cable models, including the node, the juxtaparanode, and the internode. The figure is not drawn to scale.

Previous modeling work has suggested that bending of the axon may lead to substantial depolarization at the bend, which could potentially lead to the initiation of an action potential at this point [115]. The action potential initiation was thus investigated for the models implemented in studies I and II. The models were always activated either at the nerve fiber ending or the first node of Ranvier, wherefore, the estimated activation thresholds were not affected by the bending structure of the axon or the transition between skin layers.

Peripheral nerve fibers and especially small nociceptive fibers, display substantial branching [22], [23], and thus other models with more detailed branching structures exist [20], [53]. Mørch et al. (2011) [20] proposed a stochastic nerve fiber model with a 10 % probability of branching when the nerve fiber reached the dermal skin layer. Branching occurred at the nodes of Ranvier, and for each branching, the fiber diameter was reduced. Additionally, random termination depths of the nerve fiber endings were

implemented. The model of Mørch et al. [20] was morphologically complex. However, only the passive membrane components were implemented, and activation was assumed when the membrane potential exceeded an arbitrary threshold. Having both very detailed branching and detailed active ion-channel dynamics would be too computationally demanding. Consequently, the model chosen for studies I and II was a compromise between morphological details and details of ion-channel dynamics. The ion-channel distribution has been shown to differ between nerve fiber types [120]–[123], with a great influence on the strength-duration relationship [46], [118], why a model of simplified morphology but with a wide range of ion-channels was preferred for the investigation of electrode designs for preferential small fiber activation. Furthermore, the branches of peripheral nerve fibers have been observed to have a limited integration ability [124], where the first arriving action potential blocks the action potentials from other branches. The action potential that induces perception is thereby most likely to originate from the branch whose nerve fiber ending is closest to the electrode. This suggests the spatial position of the nerve fiber ending relative to the electrode to have a stronger influence on the ability to preferentially activate nociceptive fibers than the branching structures of the nerve.

### 3.2.2. VOLTAGE-GATED ION CHANNEL DYNAMICS

The voltage-gated ion channels in the models of study I and II were Hodgkin-Huxley (HH) type ion channels. Hodgkin and Huxley were the first to present an accurate model of membrane excitability based on experimental observations of the giant axon of the squid [125]. The ion channel voltage dependency is introduced in the HH model as gating variables. For the original model of sodium currents, three activation gates and a single inactivation gate describe the opening and closing of the sodium channels. Rate constants were implemented to explain how depolarization of the membrane promotes activation and inactivation of the gates, and the gates were assumed to be independent serial gates so that the channel only conducts current when all gates are open. The potassium currents were in the original HH model described by four activation gates. Apart from the voltage-gated sodium and potassium currents, the model also included a leak current that more or less accounted for other less recognized currents and determined the resistance of the neuron. With the continued discovery of voltage-gated ion channels and channel subtypes, the HH model has been used to model a variety of channels with similar voltage-dependencies and activation-inactivation kinetics. The HH model is likely the most popular model as it is relatively simple and is able to reproduce experimental data. Additionally, the parameters of the model may be determined relatively easily from experimental data, such as patch-clamp experiments [126]. One of the assumptions of the HH model is that the currents can be described through average conductances. This is, however, a simplification and may not hold for very small structures or for sparsely expressed ion channels. The single ion channel dynamics may be more accurately explained by multistate

modeling, where Markov formalisms are used to describe the stochastic transitions between channel states [127]. However, multistate modeling is more computational demanding compared to HH modeling, and parameter estimation from experimental data is often more complicated [126]. Consequently, if the desire is to explain single-channel behavior, more complex multistate models are necessary. However, if the principal requirement for the model is to generate action potentials and estimate nerve fiber activation thresholds, the more simple HH model approach is sufficient.

The differences in the expression of voltage-gated ion channels between large and small fibers have been suggested to account for the observed excitability differences. The chronaxie of the strength-duration relationship has been observed to be lower for large fibers compared to small fibers [26][26], [42], [128], [129]. The voltage-gated ion channel kinetics are essential to the nerve fiber response and excitability, and a higher fraction of fast-activating sodium channels has been related to decreased chronaxie values [46]. Furthermore, perception thresholds vary differently for large and small fibers with the duration of slowly depolarizing pulses [26], [47] as well as hyperpolarizing prepulse [42]. This behavior has been suggested to be related to the fractional differences in persistent sodium channels that display slow inactivation dynamics [42], [46]. A higher fraction of persistent sodium increases chronaxie values [118] as well as the nerve fiber excitability to long hyperpolarization prepulse and long slowly rising depolarizing pulses [46]. The TTX-resistant ( $\text{Na}_{\text{TTXr}}$ ) channels  $\text{Na}_v1.8$  and  $\text{Na}_v1.9$  are likely to be involved in the difference in excitability to slowly increasing depolarizing pulses between large and small fibers as these channels are predominantly expressed in small diameter nociceptors and display slow inactivation kinetics [47], [120]. Additionally, there is a difference in the expression of TTX-sensitive ( $\text{Na}_{\text{TTXs}}$ ) sodium channels between large and small fibers. The main  $\text{Na}_{\text{TTXs}}$  channel in large fibers is  $\text{Na}_v1.6$ , whereas the concentration of this channel is relatively low in small fibers [120]. In small fibers, the main  $\text{Na}_{\text{TTXs}}$  channel is  $\text{Na}_v1.7$ . The kinetics of activation and inactivation of these two channels are distinct, especially in relation to the closed state inactivation, which is slower for  $\text{Na}_v1.7$ , allowing some channels to remain open during slow ramp currents [120].

The knowledge on differences in distinct kinetics and expressions of potassium channels between small and large fibers is not as elaborate. Nevertheless, the distribution has been shown to vary in sensory fibers [121]. Additionally, slow potassium currents have been proposed to be highly involved in the increased nerve fiber excitability to slowly depolarizing pulses, which is mainly observed in large fibers [118].



The nerve fiber models implemented in studies I and II were developed specifically to describe the excitation differences observed between small and large fibers and therefore included differences in ion channel expression. The implemented voltage-gated ion channels in the A $\beta$ -fiber model included the Na<sub>v</sub>1.6, K<sub>dr</sub>, K<sub>M</sub>, K<sub>A</sub>, and the HCN channel. The A-beta fiber model included the same channels and three additional channels; Na<sub>v</sub>1.7, Na<sub>v</sub>1.8, and Na<sub>v</sub>1.9.

### 3.3. MODEL SIMULATIONS

#### 3.3.1. ELECTRODE IMPEDANCES

At low frequencies, the impedance is dominated by the electrode resistance and would, in the ideal case, lead to a somewhat constant impedance response [130]. As the stimulation frequency is increased, the electrode capacitance begins to dominate the impedance resulting in a decreasing impedance with increasing frequencies [131], [132]. Consequently, both conductivity and permittivity are necessary to be able to characterize the complex impedance throughout the entire frequency range. For impedance measurements, the electrical potential is usually time-harmonic, why a frequency-domain simulation was used to estimate electrode impedance. The assumption of time-harmonic behavior makes it possible to completely eliminate time as a variable in the equations. Instead, the angular frequency is introduced as a parameter. Thereby, for a frequency-domain simulation, the time-harmonic equation of continuity (see equation 3.11) is solved.

$$-\nabla \cdot ((\sigma + j\omega\varepsilon_0\varepsilon_r)\nabla V - J_e) = 0 \quad 3.11$$

Where  $V$  is the electrical potential,  $\sigma$  is the material conductivity,  $\varepsilon_r$  is the relative permittivity of the material,  $\varepsilon_0$  is the permittivity in vacuum and  $J_e$  is the externally applied current density.

The output of the frequency domain simulation is a complex quantity and may thus be divided into magnitude and phase angle.

#### 3.3.2. TIME DEPENDENCY

It was clear from the frequency domain study that the inclusion of the tissue permittivity was important to gain reliable simulations for the impedance response. Consequently, a time-dependent simulation was conducted to evaluate the effect of the capacitive properties of the skin when stimulating with rectangular pulse shapes as used for determining strength-duration curves. The models of the intra-epidermal

and planar concentric electrodes were used for the analysis. The simulation revealed a very limited effect of pulse duration on the maximum electrical potential, which would not affect the nerve fiber activation (illustrations of the time-dependent simulation results can be found in the supplementary material of study I). The fast rise time of rectangular pulse shapes results in an equally fast rise in the electrical potential and makes a quasi-static simulation adequate when estimating nerve fiber activation thresholds. For stimulation pulses of shorter durations or different shapes, such as sinusoids or slowly rising currents, a time-dependent study would be necessary.

### **3.3.3. AREA OF SELECTIVITY**

The objective of the area of selectivity was to quantitatively describe where within the volume conductor small fibers could be selectively activated. Combined with the normal values of epidermal nerve fiber density, the area of selectivity may, additionally, provide an estimate of the amount of selectively activated small fibers. The area of selectivity was defined in the x-y plane as the area within which a lower activation threshold could be achieved for the A $\delta$ -fiber model than for the A $\beta$ -fiber. The estimation of this area was performed through an iterative search that is described in studies I and II and illustrated in Figure 3.3 and Figure 3.4. In the previous modeling works, a marching cube algorithm has been used to estimate the volume within which nerve fibers were activated [133]. This algorithm is, however, more computationally demanding, and several additional nerve fiber model evaluations would be needed to achieve an accurate estimation. With the complexity of the nerve fiber model, this would drastically increase the computational time.

### Illustration of calculation of area of selectivity

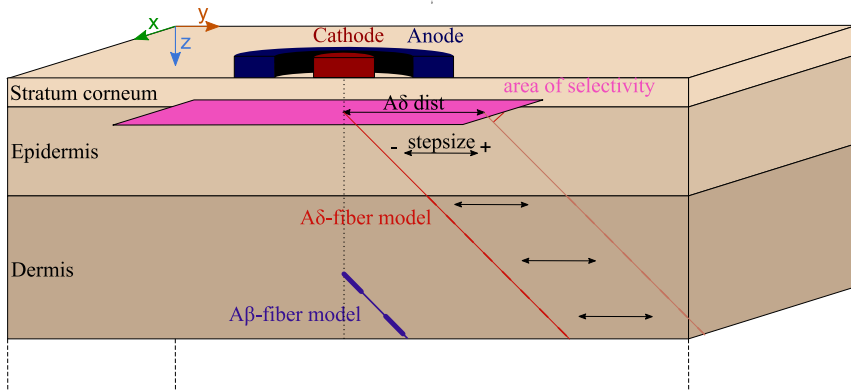


Figure 3.3: Illustration of the calculated area of selectivity.

### Flowchart for calculating the area of selectivity

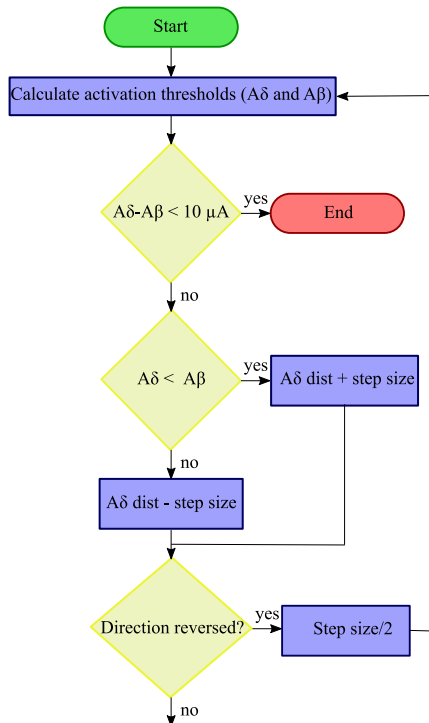


Figure 3.4: Flowchart of the procedure for determining the area of selectivity.

### 3.3.4. STRENGTH-DURATION CURVE

Simulations of the strength-duration curve were made by calculating the activation threshold of the nerve fiber models for rectangular stimulation pulses of different durations [21]. Since the action potentials within the models were initiated in the nerve fiber branch, with the tip closest to the center of the cathode, the location of the nerve fiber relative to the cathode was considered of great importance. Consequently, to catch the possible variation in the nerve fiber activation threshold caused by nerve fiber location, multiple strength-duration curves were estimated for 12 random locations. The area of selectivity determined the space within which  $A\delta$ -fiber model locations were picked. For the z-direction, the depth of nerve fiber termination was randomly picked in the range 21-61  $\mu\text{m}$ , from just below the junction between the stratum corneum and epidermis to the middle of the epidermal skin layer. The total volume of possible locations around a single cathode for the  $A\delta$ -fiber model was 0.003  $\text{mm}^3$ , 0.09  $\text{mm}^3$ , 0.032  $\text{mm}^3$ , and 0.006  $\text{mm}^3$  for the pin, planar array, planar concentric, and intra-epidermal electrodes, respectively. For the patch, which did not exhibit an area of small fiber selectivity, the volume was 0.452  $\text{mm}^3$ , restricting the nerve fiber location in a radius of 0.6 mm in the x-y plane. The volume of possible locations of the  $A\beta$ -fiber model was 0.09  $\text{mm}^3$  and was the same for all electrodes. The  $A\beta$ -fiber model location was picked within a radius of 600  $\mu\text{m}$  from the cathode center within the x-y plane, while it for the z-direction was  $\pm 40$   $\mu\text{m}$  relative to the original position in the middle of the dermal skin layer.

### 3.3.5. GLOBALIZED BOUNDED NELDER-MEAD OPTIMIZATION

Since the existing electrode designs for preferential small fiber activation have all been developed empirically, there are likely subspaces of the electrode dimension space that have not been investigated. Thereby, there could be a potential for improvement of the electrode performance. Combining the computational model with an optimization scheme makes it possible to search through large solution spaces in a systematic and time-efficient manner.

A globalized bounded Nelder-Mead (GBNM) algorithm, as introduced by Luersen et al. [134], was used for the optimization [24] (see flowchart in Figure 3.5). The Nelder-Mead algorithm is a well-known and often used gradient-free optimization method [135], [136]. It does, however, display some weak points that are addressed in the GBNM approach by the addition of restarts. In the original Nelder-Mead algorithm, the simplex may collapse and thereby be unable to escape a specific subspace of the solution space [135]. The GBNM algorithm introduces a restart scheme to overcome this issue, where a new simplex is initialized based on the current best vertex [134]. Furthermore, the original algorithm may terminate prematurely due to insufficient progression [135]. This was likewise handled by restarts in the GBNM algorithm.

Probabilistic restarts were initiated whenever the local search has converged and repeated the local search until 20 restarts had been performed [134]. This decreased the error introduced by a premature termination and additionally increased the probability of locating a global optimum [134]. Lastly, the GBNM algorithm introduced bounds within the algorithm that were used to constrain the search space within the predefined upper and lower bounds for the investigated electrode parameters (see Figure 3.6). The objective function to maximize was the activation threshold ratio between the two nerve fiber models. Optimization was performed for each parameter individually, while keeping the remaining parameters constant.

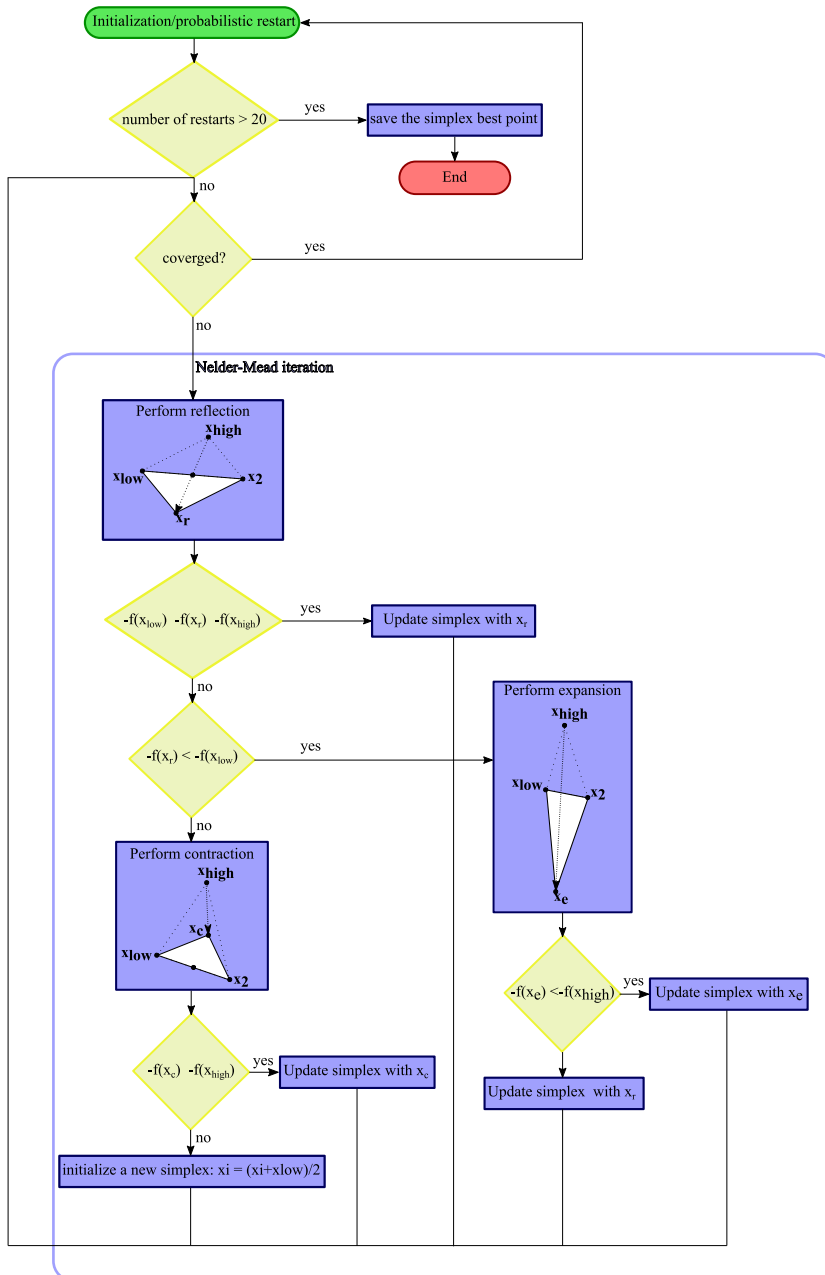


Figure 3.5: Flowchart of the Globalized Bounded Nelder Mead (GBNM) algorithm used in study II [24]. Three runs were performed for each parameter with random initialization of the simplex.

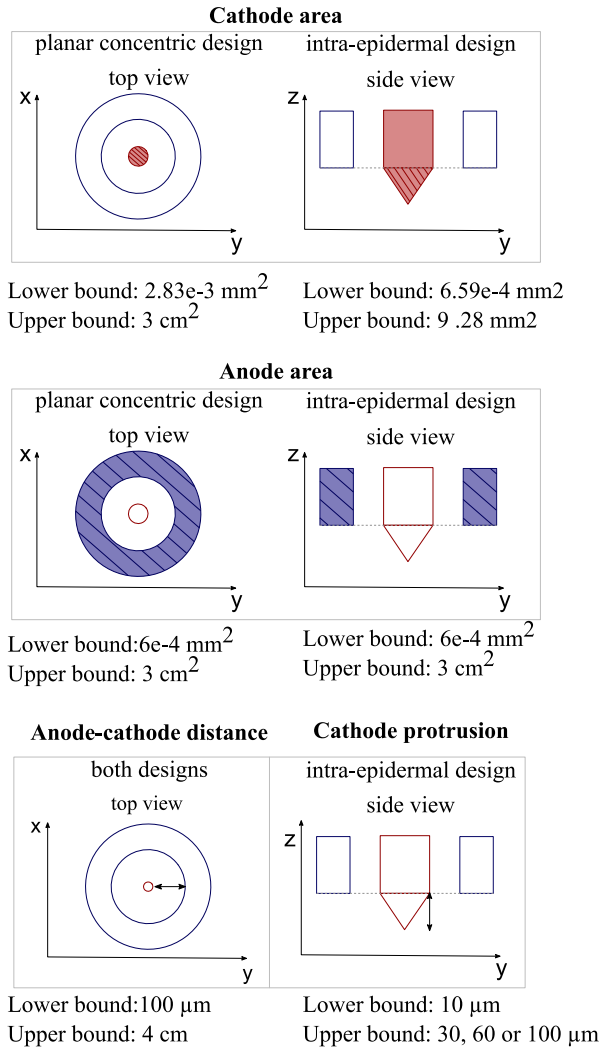


Figure 3.6: Illustration of the electrode parameters investigated in the optimization (study II) and the lower and upper bounds used to restrict the range of the solution space. Sketches of electrode parameters are modified from study II [24], and not drawn to scale. © IOP Publishing, reproduced with permission. All rights reserved.

### 3.4. MODEL SENSITIVITY

The sensitivity of the volume conduction model was evaluated by determining the change in the simulated results by varying the values of the skin layer thickness, conductivity, and permittivity from maximum and minimum values observed in previous literature (see values in Table 3.1 ). The input parameters were tested one at a time while keeping the remaining parameters constant. The sensitivity analysis was performed for the planar concentric, intra-epidermal, and patch electrodes, representing the main variations in electrode design. Parts of the results are reported in study II, where the sensitivity to conductivity changes was investigated for the planar concentric and intra-epidermal electrode designs.

For the nerve fiber excitation model, the sensitivity to the nerve fiber location was evaluated by the simulations of the strength-duration curve and the estimation of the area of selectivity, for which simulations of the A $\delta$ -fiber model were performed at different locations. The nerve fiber location was considered a key feature as the models were activated at the nerve fiber ending or at the first node of Ranvier, and limited integration has been observed for nociceptive braches [124]. The first arriving action potential usually blocks the action potentials from other branches by collision [124], and thereby, the action potential that leads to perception most likely originated at the fiber branch with the tip closest to the electrode.

#### 3.4.1. SKIN THICKNESS

The thickness of the stratum corneum mainly influenced the distribution of the electrical potential and the nerve fiber activation for the small area electrodes. The largest effect was observed for the planar concentric electrode, for which the maximum change in the activation threshold ratio between the nerve fiber models was a 38 % increase when the stratum corneum had a thickness of only 11.27  $\mu\text{m}$ . For the epidermis, an increase in thickness resulted in an increased activation threshold for both nerve fiber models. However, the increase was larger for the A $\beta$ -fiber model, and thus, the maximum increase in activation threshold ratio was 18.8 % and observed for the intra-epidermal electrode. Naturally, the dermal thickness did not affect the A $\delta$ -fiber activation as the nerve fiber remained in the same position relative to the electrode. The A $\beta$ -fiber model, on the other hand, was located further away for increased thicknesses and thus displayed increases in the activation threshold. The changes in the nerve fiber activation thresholds were larger for the small area electrodes compared to the patch, which was expected due to the extensive current spread generated by the patch.

The electrode impedance was mainly affected by the thickness of the stratum corneum, and the change was largest for the intra-epidermal electrode (75.14 %). This



was not surprising as the needle went from penetrating the stratum corneum by 10  $\mu\text{m}$  to only just reaching the junction between the stratum corneum and the viable epidermis.

### 3.4.2. SKIN LAYER CONDUCTIVITY

The sensitivity analysis of the skin layer conductivity is partly reported in study II for the planar concentric and intra-epidermal electrodes. The conductivity of the stratum corneum had a limited effect on the nerve fiber activation but quite a large effect on the electrode impedance. The impedance response of the patch electrode clearly showed the influence of the stratum corneum in the low-frequency range. For the minimum conductivity, the impedance displayed similar features to that in the implemented model with high impedance in the low-frequency range and a decrease to a plateau at high frequencies. However, for the high conductivity of the stratum corneum, the impedance was almost constant throughout the entire frequency range. The maximum change in impedance was observed for the intra-epidermal electrode (99 %), and the impedance decreased with increasing conductivity. High effect on impedance but limited effect on nerve fiber activation for stratum corneum conductivity even for the planar electrodes could be due to the thin thickness of the stratum corneum layer. For increased thicknesses, the model would be expected to be more sensitive to conductivity changes of the stratum corneum. The nerve fiber activation was mostly affected by changes within the skin layer of termination. Thus the A $\delta$ -fiber activation was more sensitive to changes in the epidermal conductivity, and the A $\beta$ -fiber model was most sensitive to changes in the dermal conductivity. The maximum changes in the activation threshold ratio were observed for the intra-epidermal electrode and were 15 % and 21 % for the epidermal horizontal and dermal horizontal conductivity, respectively. Altering the conductivity of the hypodermis did not affect the simulation results for the small area electrodes. For the patch electrode, the activation thresholds changed by approximately 10 %, however, leading only to minor changes in the activation threshold ratio ( $\sim$ 1 %).

### 3.4.3. SKIN LAYER PERMITTIVITY

The capacitive properties of the skin tissues were only accounted for when simulating the electrode impedance response, why the activation thresholds of the nerve fiber models were not considered for the sensitivity analysis of the tissue permittivity. The permittivity of the stratum corneum had a large influence on the impedance response, especially for frequencies within and above the kHz range. The greatest change was observed for the intra-epidermal electrode and the low permittivity (74 % decrease in impedance at approximately 2.5 kHz). The maximum change in impedance for the

epidermis was observed for the planar concentric electrode in the high-frequency range (14 %). The permittivity of the dermis and hypodermis did not affect the overall electrode impedance.

#### 3.4.4. NERVE FIBER LOCATION

The spatial distribution of the electrical field produced by the electrode determines the activated population of nerve fibers. Thus, the location of the nerve fiber relative to the electrode has a great influence on the activation threshold. The small area electrodes were most sensitive to nerve fiber location. For the intra-epidermal electrode, the activation threshold difference between the lowest and highest threshold estimates was 2.2-5.6 mA for the longest and shortest pulse duration, respectively. For the planar concentric electrode and the pin electrode, the differences were between 0.35-3.0 mA and 0.3-0.5 mA, respectively. The cathode area of the pin is smaller than for the planar concentric electrode, and thus, greater variations could have been expected for the pin electrode. However, the multiple cathode design of this electrode is likely to decrease the electrode sensitivity towards nerve fiber location. Small differences were observed for the patch electrode, where the maximum difference in activation threshold was 0.04 mA for the shortest pulse of 0.1 ms. This is in agreement with the estimated area of selectivity in studies I and II. From these estimates, it was clear that the ratio between the activation threshold of the two nerve fiber models increased for smaller electrode areas. However, the area of selectivity became narrower, indicating that the electrode must be positioned in close proximity to a nerve fiber ending to achieve small fiber preferentiality. This imposes practical issues for the electrode used, and the electrode may have to be re-positioned several times before placement with an acceptable perception threshold is achieved [32], [137]. Thereby, merely placing the electrode may become a cumbersome task. However, the depth for which preferential activation of the A $\delta$ -fiber model could be achieved increased with decreased electrode area, suggesting that deeper-lying small fibers may be activated at a lower threshold than large fibers when small area electrodes are used. Furthermore, the small area electrodes produced more uniform areas of selectivity for different nerve fiber termination depths, whereas the area of selectivity greatly decreased with nerve fiber depth for larger electrode areas. This opportunity to preferentially activate deeper epidermal nerve fibers may be of special interest in the assessment of small fiber neuropathy as the intra-epidermal nerve fibers have been shown to degenerate resulting in fewer and shorter intra-epidermal nerve fibers [138], [139]. In order to keep the improved selectivity of small fibers and the possibility to activate deeper epidermal nerve fibers preferentially, without the practical issues of electrode placement, electrode designs with multiple cathode or anode-cathode pairs may be used.

### 3.5. MODEL LIMITATIONS

#### 3.5.1. SIMPLIFICATIONS AND LIMITATION OF THE VOLUME CONDUCTION MODEL

Simplifications were made to the geometry of the skin model. Several structures, such as appendages, sensory receptors, and vascular structures, were omitted in the model, and variations in water content within the skin were not considered. Additionally, the dermal-epidermal junction is known to have a papillary structure to increase the effective area of nutritional transport [60] but was modeled as a straight horizontal junction.

The blood has a larger conductivity than skin tissue and therefore may act as a current shunt and affect the potential distribution in their proximity [140]. The larger the vessels, the larger the effect on current spread [140]. The blood vessels of the skin are located in the dermis and hypodermis in horizontal plexuses, from which they spread out, and small capillaries supply the papillary dermis [60]. The inclusion of the complex structures of the blood vessels was not expected to influence the small fiber activation due to the activation point at the tip of the model and due to the model location in the avascular epidermis. Likewise, the blood vessels in the dermis are relatively small and therefore not expected to influence nerve fiber activation.

Appendage structures in the skin may greatly affect the current spread and potential distribution in the skin during electrical stimulation. Typically, the highest current densities are produced in the proximity of sweat ducts and hair follicles, as they establish low impedance pathways for electrical currents and allow the current to reach deeper-lying structures. High current density in the vicinity of the junctions between skin layers can be observed near sweat ducts [52]. The presence of skin appendages under the electrode may, thereby, reduce or completely eliminate the possibility to preferentially activate small fibers. The density of sweat ducts in the skin of the forearm is approximately 1.04 per mm<sup>2</sup> [141], while the size of the glands is between 50 and 100  $\mu\text{m}$  [103], [142]. With smaller electrodes, the probability of placing the electrode on top of a sweat duct decreases, and for needle-shaped designs, it becomes very unlikely. Apart from the location of the electrode relative to the sweat duct, the location of the nerve fiber relative to the sweat duct is also relevant, as the inhomogeneity that the sweat duct constitutes may only affect nerve activation within specific proximity [52]. Likewise, inhomogeneities in the skin, such as varying water content, may affect the conductivity properties of the skin and thereby the current distribution and the resulting nerve fiber activation [103]. The effect of such skin inhomogeneities tends to be rather small for small area electrodes and may for larger electrodes be minimized by high resistivity hydrogels [103].

### **3.5.2. SIMPLIFICATIONS AND LIMITATIONS OF THE NERVE FIBER MODEL**

The nerve fiber models were merely a representation of the average nerve fiber population, and thus the results should be considered a population mean. Different diameters and trajectories were not investigated. The inclusion of a wide variety of model diameters was considered too computationally demanding and time-consuming as the voltage-gated ion channel conductances would need to be rebalanced for each diameter. The model was, however, still able to reproduce experimental outcomes, likely, due to the initiation site of the action potentials.

### **3.6. MODEL VALIDATION**

In study I, verification of the model was performed by comparing simulation results to experimental data obtained for 15 healthy volunteers [21]. Ideally, each of the modeling steps and the combined model would be verified. However, getting experimental verification for the current distribution in the skin and to directly measure nerve fiber excitability is difficult and/or cumbersome, and often more indirect measures are used.

#### **3.6.1. IMPEDANCE**

Direct measures of the current density within the skin at different depths would be ideal for validating the volume conduction model and could potentially be achieved by current density imaging. Current density imaging utilizes specialized magnetic resonance imaging (MRI) protocols to enable measurements of the magnetic fields produced by current flow in the tissue and subsequently calculate corresponding current densities [143]–[145]. Current density imaging has previously been shown to correspond well to finite element model estimations of the current distribution under large area electrodes [143], [144]. However, it is a rather complicated, time-consuming, and expensive method that demands MRI-compatible stimulation electrodes as well as highly qualified and experienced personnel. Furthermore, to generate measurable magnetic fields, high currents are required [145], which is not considered feasible for the small area electrodes developed for small fiber activation. A more simple, fast, and inexpensive way to validate the volume conduction model is to compare simulated and experimentally measured electrode impedances. By applying a low amplitude current (usually below perception threshold) at the cathode and recoding the voltage received at the anode, the impedance magnitude and phase may be calculated. The impedance measurement will at the low frequencies be largely dominated by the electrode-skin interface, however, when the frequency becomes

high enough, the electrode capacitance is shorted, and the skin impedance becomes visible as a plateau in the impedance spectrum [132], [146]. Comparing the simulated impedance with experimental measurements thus compose a verification of the volume conduction model of both the electrode-skin interface and the skin. This method is, however, an indirect validation as it can only assess the sum of skin layer impedances and cannot distinguish between the skin layers or verify model estimated current densities at different depths.

The simulated impedance of the electrodes corresponded well to the experimental data. The relative contribution for the electrode-skin interface and the skin was best observed for the patch electrode, where the impedance reached a plateau around 30 kHz. The bulk skin impedance based on the patch measurements was approximately 500  $\Omega$ , agreeing with that estimated in the model 463.1  $\Omega$ .

### 3.6.2. NERVE FIBER EXCITABILITY

The model predictions of the combined volume conduction and nerve fiber model may be verified by comparing simulated nerve fiber activity with experimental recordings of peripheral nerve responses. The activity of large diameter fibers can be recorded as compound action potentials [147]. The applied electrical stimulation synchronizes nerve fiber recruitment and activity, and the sum of the action potentials of activated fibers may be recorded over the nerve trajectory [147], [148]. However, recording small fiber activity is a more challenging task as measurements of compound action potentials generated from small fibers are infeasible [147]. Microneurography may be used to record small fiber activity. However, this technique is cumbersome and demands experienced personnel. Instead of measuring the nerve fiber activity directly, the perception threshold may provide an indirect measure of the nerve fiber membrane properties [42]. As an indirect measure, it is important to realize that the perception threshold is not only dependent on the peripheral activity but is also influenced by central processing. The contribution of the peripheral and central nervous systems is thus difficult to disentangle. Nevertheless, measurements of threshold electrotonus and strength-duration curves have displayed similar patterns for perception thresholds as for compound action potentials [42], [118], [129], [149], suggesting that the main contributor to the perception threshold is of peripheral origin.

By determining the perception threshold to rectangular stimulation pulses of different durations, it is possible to quantify the strength-duration relationship and calculate the rheobase and chronaxie values, providing insights into the nerve fiber excitability [97]. The rheobase is highly dependent on the distance to the source of stimulation [150]. Longer distances will result in higher rheobases. The general shape of the strength-duration curve is, however, not affected by distance, and the chronaxie is expected to remain the same [150]. Large mechanical nerve fibers are more excitable

and exhibit faster conduction velocities compared to small nociceptive fibers, and therefore display shorter chronaxie values. Consequently, the strength-duration relationship can be used to distinguish between fiber types and verify which fibers are activated for a specific electrode design. It is, however, important to notice that tissue homogeneity is assumed when determining the chronaxie and that the chronaxie estimate is sensitive to the experimental design, electrode, and stimulator properties [150].

Experimental estimations of chronaxie values in studies using surface electrodes are presented in Table 3.2, from which considerable variations between studies can be observed. The chronaxie of small fibers has been estimated to be between 435  $\mu\text{s}$  and 4,650  $\mu\text{s}$  [26], [128], [129], [151], [152], while it for large fibers has been estimated to be between 257 and 665  $\mu\text{s}$  [26], [128], [129], [151], [153].

Table 3.2: Chronaxie values for small and large fibers found in the literature.

Reference	Small fiber chronaxie (Pin/intra-epidermal electrode stimulation)	Large fiber chronaxie (Patch electrode stimulation)
Hennings et al. [42]	1,060 $\pm$ 690 $\mu\text{s}$	580 $\pm$ 160 $\mu\text{s}$
Hugosdottir et al. [26]	4,560 $\mu\text{s}$ (IQR 7,170 $\mu\text{s}$ )	570 $\mu\text{s}$ (IQR 107 $\mu\text{s}$ )
Hoberg et al. [129]	547 $\mu\text{s}$ (IQR 470-648 $\mu\text{s}$ )	257 $\mu\text{s}$ (IQR 216-344 $\mu\text{s}$ )
Hugosdottir et al. [128]	1,330 $\mu\text{s}$ (IQR 2,040 $\mu\text{s}$ )	590 $\mu\text{s}$ (IQR 190 $\mu\text{s}$ )
Doll et al. [154]	435 $\mu\text{s}$	X
Mogyoros et al. [153]	X	665 $\pm$ 182 $\mu\text{s}$

In study I, the simulated strength-duration curves verified the model predictions [21]. However, the model did predict a lower chronaxie for the large patch electrode compared to what was observed experimentally. The model chronaxie was estimated only for the nerve fiber model that achieved the lowest activation threshold, whereas experimental measurements are likely derived from a combined activity of both fiber types.

### 3.6.3. SKIN THICKNESS

Apart from the reported outcome measures in study I. [21], skin thicknesses were determined and compared to the values implemented in the model. Skin thickness was accessed for comparison with the implemented thicknesses of the model. As the sensitivity analysis showed that the stratum corneum thickness is of great influence, especially for small area electrodes, and when simulating the skin impedance, this skin layer was accessed individually by tape stripping and measurements of trans-epidermal water loss (TEWL). The combined thickness of the epidermis and dermis was quantified through ultrasound recordings.

#### 3.6.3.1 Stratum corneum thickness

Exact measurement of the stratum corneum thickness is difficult to obtain in a completely non-invasive way. One relatively simple and accessible way of estimating the stratum corneum thickness *in vivo* is to utilize the relationship between the TEWL and the thickness of the removed stratum corneum through tape stripping [155]. By performing tape stripping, layers of the stratum corneum were gradually removed, and TEWL was measured, with a DermaLab TEWL open-chamber probe by *Cortex Technology (Cortex Technology ApS - Denmark)*, after every five strippings. The tape stripping was terminated when the TEWL value had increased to 3-4 times the original value or until glistening spots were detected on the skin surface. The thickness of the stratum corneum was estimated by the baseline-corrected non-linear model presented by Russell et al. [155] (See equation 3.12).

$$TEWL_x = B + \frac{D \cdot K \cdot \Delta C}{H - x} \quad (3.12)$$

Where  $TEWL_x$  is the TEWL after x tape strippings, B is the TEWL at baseline, D is the diffusion coefficient of water within the stratum corneum, K is the tissue partition coefficient of water,  $\Delta C$  is the water concentration gradient, and H is the thickness of the removed stratum corneum.

The thickness of the stratum corneum was estimated to be  $22.53 \pm 12.77 \mu\text{m}$  and thus corresponded well with the stratum corneum thickness of  $20 \mu\text{m}$  implemented in the model.

### **3.6.3.2 Combined epidermal and dermal thickness**

Ultrasound is a simple and non-invasive method that may be used to measure both the epidermis and the dermis skin layer thicknesses. Separating the epidermis from the dermis can, however, be difficult and demands both high-resolution equipment and experienced personnel [100]. Consequently, the combined epidermis and dermis thickness was measured by ultrasound recording of the volar forearm. The skin thickness was measured three times on each arm and subsequently averaged. The average thickness was  $1442 \pm 218 \mu\text{m}$ , which corresponded well with the value of the combined skin thickness of the stratum corneum, viable epidermis, and dermis used in the model ( $1402 \mu\text{m}$ ).



# CHAPTER 4. A NOVEL ELECTRODE DESIGN

## 4.1. OPTIMIZED ELECTRODE DIMENSIONS

In study I, the intra-epidermal and the planar concentric electrode designs displayed the largest activation threshold ratio between small and large fibers. Therefore, these two electrode designs were used in the optimization of study II. Original and optimized electrode dimensions and their resulting nerve fiber activation are summarized in Table 4.1. It was found that the dimensions of the electrode should be minimized to achieve a nerve fiber activation as preferential towards small fibers as possible (see Figure 4.1). The protrusion of needle electrodes should preferably be designed according to the termination depth of the target fibers [24], [51]. Furthermore, the small fiber preferentiality increased more when combining all optimized electrode parameters compared to each parameter optimized individually. The obtainable increase in activation threshold ratio depended on the nerve fiber termination depth, displaying the greatest increases in the superficial epidermis (see Figure 4.2).

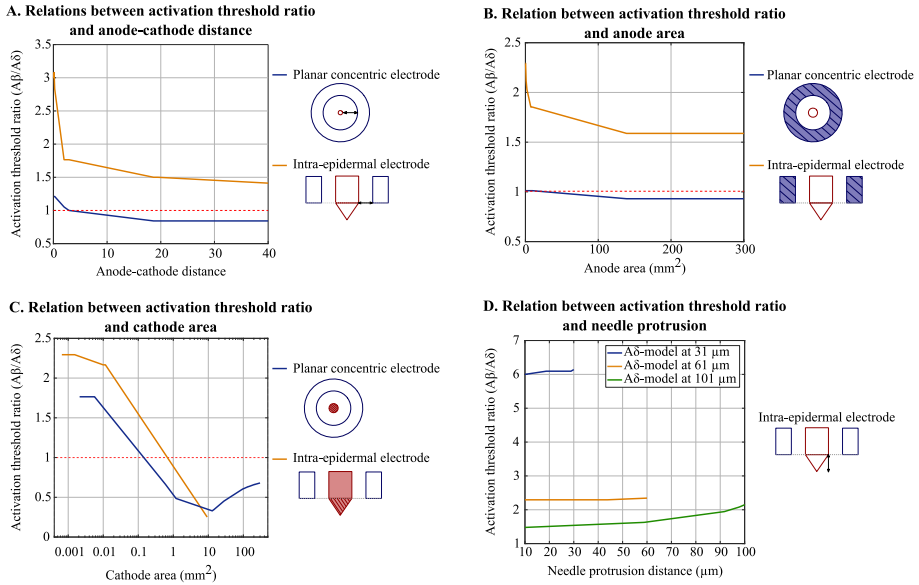


Figure 4.1: Activation threshold ratios between the two nerve fiber models at different dimensions of investigated electrode design parameters. Sketches of electrode parameters are modified from study II [24] and not drawn to scale. © IOP Publishing, reproduced with permission. All rights reserved.

Table 4.1: The original and optimized electrode dimensions and the resulting activation of the nerve fiber models.

	Intra-epidermal		Planar concentric	
	Original dimension	Optimized dimension	Original dimension	Optimized dimension
<b>Cathode area</b>	1,451 $\mu\text{m}^2$	660 $\mu\text{m}^2$	0.196 $\text{mm}^2$	2827 $\mu\text{m}^2$
<b>Anode area</b>	0.56 $\text{mm}^2$	0.054 $\text{mm}^2$	7.854 $\text{mm}^2$	0.143 $\text{mm}^2$
<b>Anode-cathode distance</b>	0.5 mm	0.1 mm	2 mm	0.1 mm
<b>Needle protrusion</b>	30 $\mu\text{m}$	A few micrometers above the	-	-

	nerve fiber ending			
Activation threshold of A $\beta$ -fiber model (mA)	0.063	0.246	0.059	0.200
Activation threshold of A $\delta$ -fiber model (mA)	0.026	0.054	0.058	0.046
Activation threshold ratio (A $\beta$ -fiber model/A $\delta$ -fiber model)	2.44	4.56	1.02	4.31

Activation threshold ratio between the nerve fiber models as a function of A $\delta$ -fiber termination depth for the original and optimized electrode dimensions

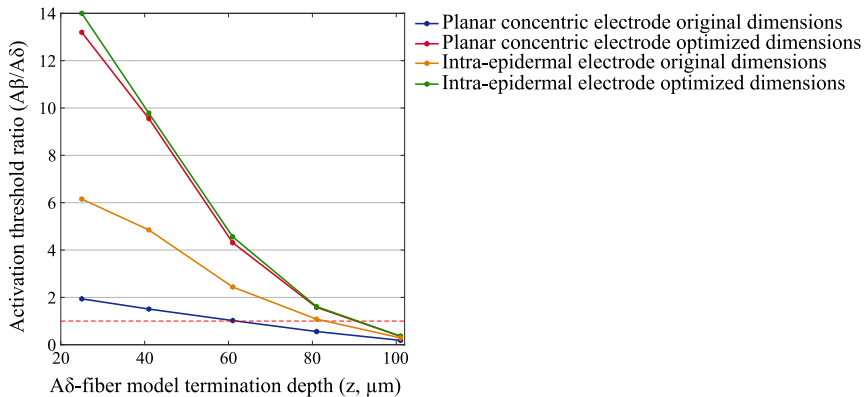


Figure 4.2: The nerve fiber activation threshold ratio between the two nerve fiber models as a function of the A $\delta$ -fiber termination depth. The stars indicate the sampled points. The dashed red line indicates nerve fiber preferentiality. Above the line, the A $\delta$ -fiber model achieved the lowest activation threshold. Below the line, the A $\beta$ -fiber model achieved a lower activation threshold than the A $\delta$ -fiber model. The activation threshold ratio, as well as the depth for which preferential A $\delta$ -fiber activation was possible, was increased when electrode dimensions were optimized.

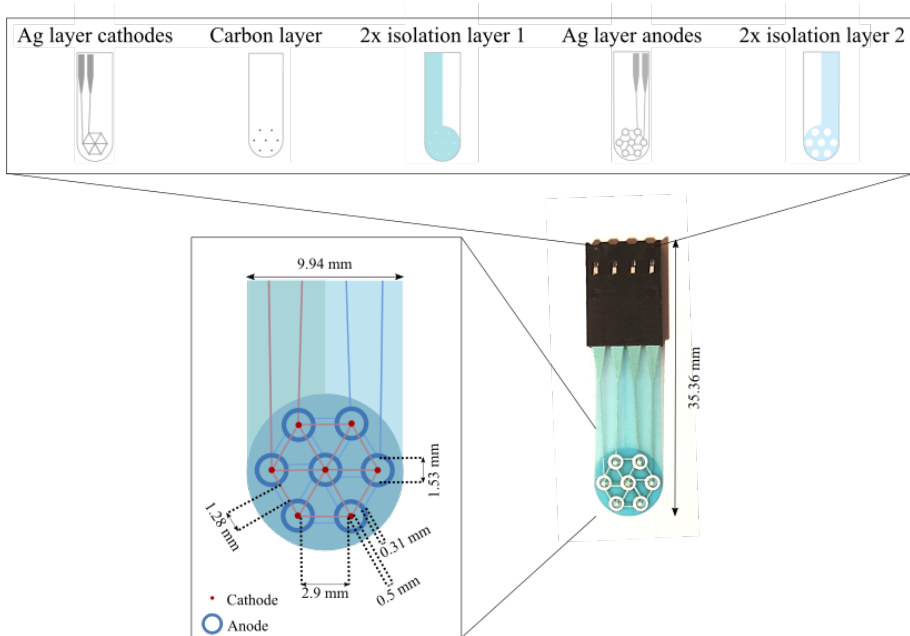
By minimizing the electrode dimensions, the current spread is confined within the epidermis, and even deep epidermal nerve fiber endings may be activated at lower

stimulation intensities than the large fibers in the dermis. However, the area within which selective A $\delta$ -fiber activation is possible also decreases with decreasing electrode dimensions, and the nerve fiber ending should lie relatively close to the center of the cathode to enable preferential activation.

## **4.2. NOVEL PLANAR CONCENTRIC ARRAY ELECTRODE DESIGN**

The electrodes with a needle design were found to be more preferential than the existing planar electrode designs. However, such electrodes are minimally invasive and need to be sterilized between uses. This costs both time and money, and if the electrode is to be used in the clinic, single-use designs are preferred. The optimization study (study II) likewise showed that planar electrodes might achieve similar preferential activation of small fibers as the needle design for very small electrode dimensions (see Figure 4.2 and Table 4.1). Consequently, a completely non-invasive and single-use planar design was chosen for the new electrode. Seven interconnected cathode-anode pairs were positioned in a hexagonal fashion to increase the effective stimulation area while still having an electrode small enough to stimulate any body part. The base of the electrode was a polyester material (PET), giving the electrode a certain degree of flexibility, allowing the electrode to follow the curvature of the body surface. Printing the electrode using conductive materials likewise made it possible to get a very thin electrode, enabling regular thermodes to be used on top of the electrode for simultaneous cooling or heating of the skin.

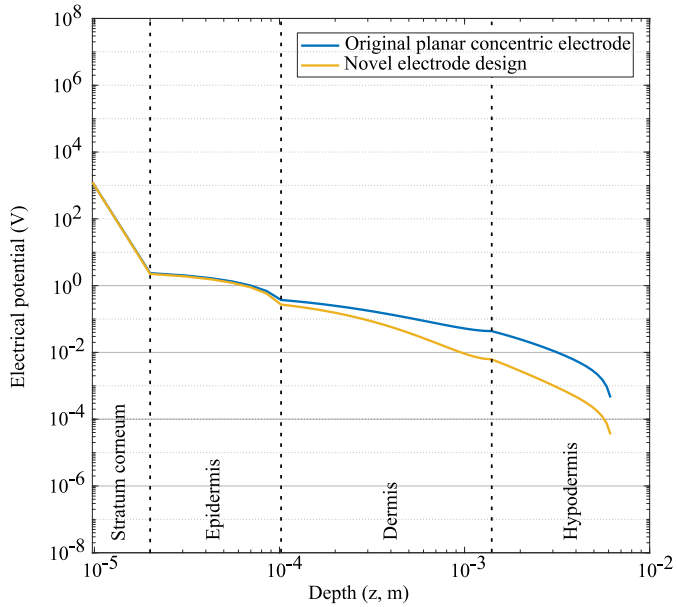
During the prototyping phase of the electrode, it was found that the electrode dimensions of study II were infeasible for printing stable electrodes, why the dimensions had to be adjusted accordingly. The final design of the new electrode is shown in Figure 4.3.



*Figure 4.3: Novel planar concentric array electrode design. The electrode base was a flexible PET material on which silver layers were printed. Several insulating layers were added between the layers of the anode and cathodes to avoid shortcutting. The electrode consists of seven interconnected concentric cathode-anode pairs positioned in a hexagonal pattern. The cathodes had a diameter of 0.5 mm. The inner diameter of the anode was 1.53 mm, corresponding to an anode-cathode distance of 0.51 mm. The width of the anode was 0.31 mm, corresponding to an outer anode diameter of 2.14 mm. The distance between the outer border of the interconnected anodes was 1.28 mm. The entire electrode had a width of 9.94 mm and a total length of 35.36 mm.*

The final dimension of the novel electrode was put into the model and compared to the computational results of the original planar concentric electrode. From Figure 4.4, it is clear that the potential within the epidermal skin layer is very similar for the original planar concentric electrode and the novel planar concentric array electrode. This is because the cathodes have the same size, and the cathode dimension is determinant for the potential in the superficial skin layers. It is likewise clear that the smaller anode of the novel planar concentric array electrode decreases the electrical potential within the dermis and thereby increases the large fiber activation threshold (see Figure 4.5). The ratio between the activation threshold of the two nerve fiber models was increased by 59.8 % for the novel electrode design compared to the original planar concentric electrode when the A $\delta$ -fiber model was located in the middle of the epidermis, and the A $\beta$ -fiber model was located in the superficial dermis.

**Comparison of the electrical potential down a straight line beneath the center of the cathode**



*Figure 4.4: The electrical potential underneath the center of the cathode, for electrode dimensions of the original planar concentric electrode and the novel planar concentric array electrode.*

## Comparison of nerve fiber activation threshold

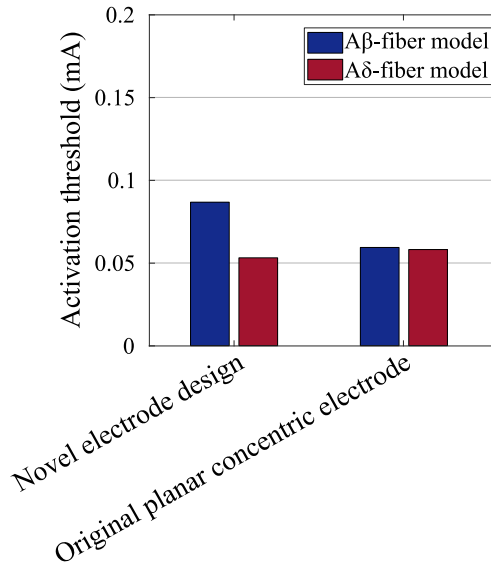


Figure 4.5: Activation threshold of the two nerve fiber models for the original and the novel electrode design.

The initial test of the novel electrode was limited to a single subject for which the strength-duration curve was assessed for both the novel electrode design, the planar concentric design, and the intra-epidermal design (unpublished data). The perception threshold was estimated for rectangular pulses of 0.5, 1, 10, 25, and 50 ms duration. Five repetitions spread out over five consecutive days were performed for each of the electrodes. The results of this simple test are visualized in Figure 4.6. The novel planar concentric array electrode provided results similar to the intra-epidermal design. The similarity was, however, not statistically quantified. The estimated chronaxies were  $0.568 \pm 0.352$  ms,  $2.459 \pm 0.132$  ms, and  $3.645 \pm 1.278$  ms for the planar concentric, intra-epidermal, and novel planar concentric array electrode, respectively.

## Test of the novel electrode design, comparison of strength-duration curves

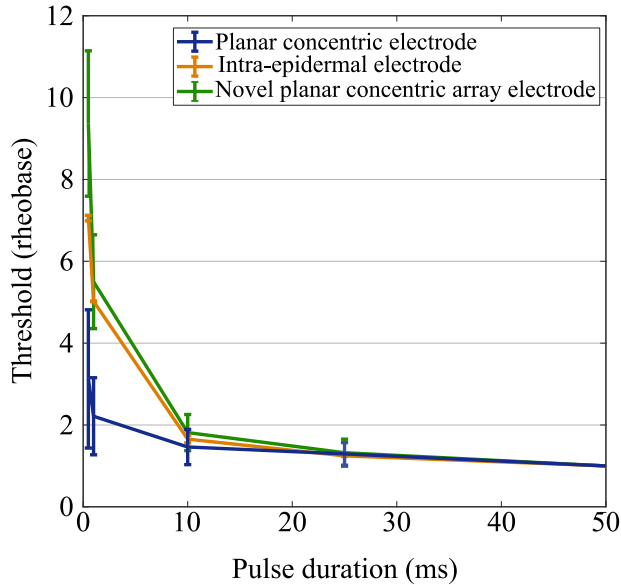


Figure 4.6: Strength-duration curves for the novel planar concentric array electrode, the planar concentric electrode, and the intra-epidermal electrode for a single subject and five repetitions. Data were obtained for a single subject with five repetitions for each of the electrodes, performed on five consecutive days.

### 4.3. PERFORMANCE OF THE NOVEL PLANAR CONCENTRIC ARRAY ELECTRODE

In study III, the performance of the novel electrode design was evaluated through measures of psychophysics, evoked potentials, and reaction times. The outcome measures were compared between a conventional patch electrode configuration known to activate large fibers and the novel planar concentric array electrode. Twenty-five healthy volunteers participated in the study. Furthermore, this section includes a comparison between the novel planar concentric array electrode with other existing electrode designs by combining the data of studies I and III.

#### 4.3.1. EVOKED POTENTIALS

Electroencephalography (EEG) measures cortical activity from surface electrodes placed on the scalp. EEG is often used to record evoked potentials (EP), defined as



the direct cortical response to an externally applied stimulus. Due to the high temporal resolution of the EEG, the EP technique has been used extensively to investigate perceptual processing to both nociceptive and non-nociceptive inputs [157]–[161]. In study III, EEG was used to record evoked potentials (EP) to electrical stimulation applied with a conventional patch electrode and the novel planar concentric array electrode. A linear mixed modeling approach was applied to account for the contribution of the different condition parameters (electrode, repetition, intensity, etc.) and for between-subject variability in the dataset [160], [162]. The generated models were used to predict the average EP (grand evoked potential prediction, GEPP) for each of the electrodes and each of the investigated stimulation intensities. In this way, the signal-to-noise ratio of the grand average EP was increased by accounting for subject variations and potentially confounding mechanisms such as habituation [162].

For the comparison between the novel planar concentric array electrode and the patch, the N1, N2, and P2 latencies were, on average, 12 ms longer for the novel planar array electrode. This latency difference may indicate a difference in the conduction velocity of activated afferents. This difference was relatively short compared to observations of Inui et al. [14] and Lelic et al. [25], who respectively compared the intra-epidermal electrode and the pin electrode to a patch-like electrode. For the EP component corresponding to the P2 definitions in the current project, Inui et al. found a latency difference between the intra-epidermal electrode and a felt tip electrode of 32.9 ms. Similarly, Lelic et al. observed a latency difference of 34.9 ms between the pin and patch electrode for the P2 component. This could potentially be explained by more preferential activation of slower conducting fibers for the intra-epidermal and pin electrode compared to the novel planar concentric array electrode. However, the P2 component of the EP is generally believed to be related to stimulus processing and may not reflect any specifics about the nature of the activated afferent fibers. Furthermore, when comparing the absolute latencies observed for the pin electrode (P2:  $248.1 \pm 29.4$  ms [25]) and the latencies of the novel planar concentric array electrode (P2: 288 ms) at corresponding stimulation intensities (10x perception threshold), the latencies were similar. For the N2 component, the latencies for the novel planar concentric array electrode were longer compared to the pin ( $148$  ms vs.  $89.5 \pm 25.3$  [25]).

A further indication of small fiber preferentiality of the novel planar concentric array electrode was the scalp map distribution, where there was a clear bilateral activity that is characteristic for nociceptive stimulation [25], [32], [158]. For non-nociceptive stimulations, the scalp maps of the early components displayed clear lateralized scalp distributions contralateral to the stimulation site [158]. In study III, such patterns were observed for the patch electrode indicating activation of large fibers.

The latencies of the EP components decreased with increasing stimulus intensity while the peak amplitudes increased. The latencies became similar to those observed by the patch electrode, which could indicate substantial co-activation of large fibers. However, the scalp distributions did not become lateralized for higher intensities. The decreased latencies could be explained by increased saliency of the stimulus facilitated by increased nociception. The EP components may be diminished or completely abolished when the saliency of stimulation is minimized by the use of short and constant inter-stimulus intervals [158]. This further suggests that these components, to a greater extent, are related to and modulated by the saliency of the stimulus rather than nociception. To that extent, it is important to note that when the subjects are asked to respond to the stimuli by pushing a button as fast as possible, this may increase the saliency and enhance brain responses reflecting higher-order cognitive functions [163]. Another possible explanation of the decreased latencies could be increased activation of fast conducting nociceptors, which has been recently described in humans [164]. These fibers are high-threshold mechanoreceptors that conduct at a similar speed as large non-nociceptive nerve fibers but induce clear painful and sharp pin-prick sensations [164].

Early components such as the N20 and the P30, which can be observed for non-nociceptive activation [158], could not be identified in study III for any of the electrodes. This was likely due to the relatively low signal-to-noise ratio and the low number of stimulus repetitions. Adding repetitions could be valuable to enable the assessment of these very early components and possibly better identify any co-activation of large fibers when stimulating with the novel planar concentric array electrode. Nonetheless, caution must be taken when adding stimulus repetitions as the observed habituation was already prominent for 30 repetitions, especially for the novel electrode design.

#### **4.3.2. PSYCHOPHYSICS**

Sensory psychophysics are used to investigate the relationship between physiological processes and sensory experiences. As it is based on subjective experiences, relatively large variations may be observed between subjects [165]. Pain scores are widely used in the assessment of clinical pain and in pain research for determining the perceived stimulus intensity for painful as well as non-painful stimuli. In study III, a numerical rating scale (NRS) was used to evaluate the perceived intensity of the stimuli. The scale ranged from 0 to 100. 0 was defined as 'No sensation,' and 100 was defined as 'Worst imaginable pain'. A score of 30 was defined as the transition from a non-painful to a painful sensation. The average NRS scores obtained for the novel planar concentric array electrode ranged from 15.3 to 28.9, being lowest for stimuli at the

level of perception threshold and highest for stimulation intensities at ten times perception threshold. The average rating did not reach the 30 point limit of the pain threshold for the high stimulation intensity. However, great between-subject variations were observed, and individual ratings for high-intensity stimulation ranged from 5 to 90. This is a good example of the subjectivity of pain perception and that it is indeed necessary to account for the random effects of the subject when analyzing this type of data. Nociceptive excitation mediating sensations of burning or pricking may not reach an alarming level to the subject and therefore may not necessarily be considered painful [165], despite its nociceptive origin. Pain perception and responses may likewise be modulated by higher-order processing such as attention and anxiety level [166]. Consequently, it is important to also assess the quality of the sensation to capture its complexity and multidimensionality. In study III the quality of the sensation was assessed by a visual analog scale anchored by the descriptors 'dull' and 'sharp' [16]. On this scale, the novel planar concentric array electrode was described to be sharp, while the conventional patch electrode was described as dull. The subjects reported clear differences in the sensation of the stimuli applied by the two electrodes, even when the NRS scores were of similar values. Furthermore, the perceived sharpness of the stimuli increased with increased stimulation intensity, which could indicate that the population of activated nerve fibers primarily consisted of A $\delta$ -fibers even for high-intensity stimulation. Had the high-intensity stimulation activated a substantial amount of large non-nociceptive nerve fibers, they would likely have contributed to the sensation, and it would have been considered more dull. Such a change in sensation was observed for stimulation through the original planar concentric electrode [41] and the micropatterned interdigitated electrode [43]. The sensation changed from pinprick to electric shock-like as the intensity was increased, which could indicate a shift in the activated nerve fiber population from preferential small fiber activation to preferential large fiber activation. It is, however, not possible to completely rule out co-activation of large fibers as the sensation mediated by large fibers could simply be masked by the nociceptive nature of the A $\delta$ -fiber activity.

#### **4.3.3. COMPARISON OF THE NOVEL PLANAR CONCENTRIC ARRAY ELECTRODE WITH OTHER EXISTING ELECTRODES**

In both studies I and III, a single rectangular pulse of 0.5 ms was used for measurements of perception threshold and simultaneous reaction time recordings. Comparing these data from study I and study III, the novel planar array electrode presented the lowest perception threshold of all investigated electrodes (see Figure 4.7). This is likely due to the fact that a higher current density is achieved within the epidermis. Furthermore, the multiple anode-cathode pair configuration is likely to activate more nerve fiber endings and thereby achieve perception at lower stimulation intensities.

### Perception threshold for a 0.5 ms rectangular pulse

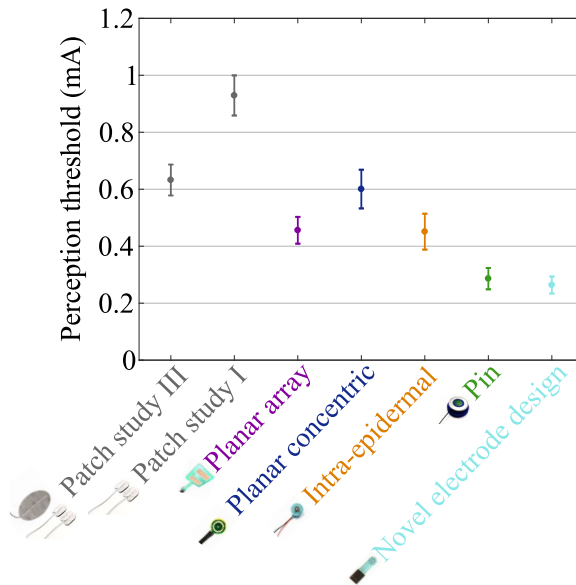


Figure 4.7: Average perception thresholds and standard errors for a 0.5 ms rectangular stimulation pulse for different electrode designs. Data on the Patch study I, Planar array, Planar concentric, Intra-epidermal, and Pin electrode are from study I, including 15 subjects. The data on the Patch study III and Planar concentric array electrodes were obtained in study III, containing data from 25 subjects. Electrode images of the patch, planar array, planar concentric, intra-epidermal and pin electrode are modified from study I [21]. © IOP Publishing, reproduced with permission. All rights reserved.

The reaction times of the novel planar concentric array electrode design were similar to the reaction times observed for the other small fiber preferential electrodes (see Figure 4.8) and were within the expected range of A $\delta$ -fiber activation (300-650 ms [32], [167]). However, reaction times do not simply reflect nerve fiber conduction velocity and are influenced by factors such as stimulation intensity, attention, motor execution, and higher-order cognitive processing for decision making [168]–[171]. Several of the subjects indicated that they were sometimes unsure whether they felt a stimulation pulse or not, which may suggest longer decision processing for stimulation intensities around the perception threshold. This may also explain the relatively high reaction times observed for the conventional patch electrode settings. It was clear in study III that the reaction times decreased with increased stimulation intensity, similar to previous observations [29], [172], [173].

### Reaction times for a 0.5 ms rectangular pulse

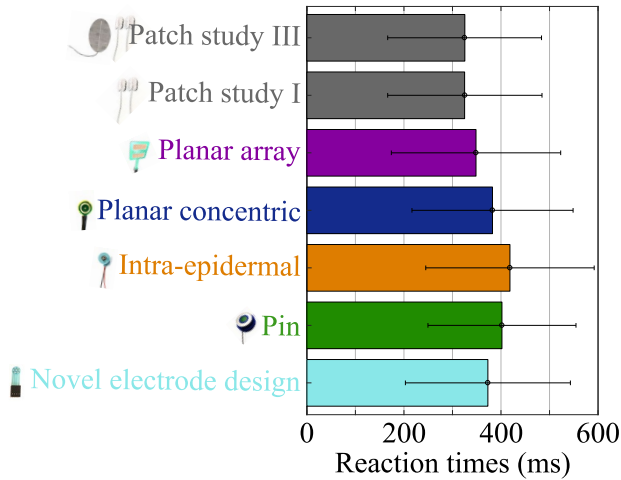


Figure 4.8: Median reaction times and interquartile range for a rectangular stimulation pulse of 0.5 ms duration for different electrode designs. Data on the Patch study I, Planar array, Planar concentric, Intra-epidermal, and Pin electrode are from study I, including 15 subjects. The data on the Patch study III and Planar concentric array electrodes were obtained in study III, containing data from 25 subjects. Electrode images of the patch, planar array, planar concentric, intra-epidermal and pin electrode are modified from study I [21]. © IOP Publishing, reproduced with permission. All rights reserved.



# CHAPTER 5. CONCLUSIONS AND FUTURE PERSPECTIVES

## 5.1. CONCLUSION

Computational modeling of electrical stimulation of the skin was utilized in a systematic framework to improve the electrode design for preferential small fiber activation. In study I, the model was implemented and validated through existing electrode designs. The model corresponded well to experimental measures of impedance and strength-duration curves.

Optimization was performed in study II, by which specific contributions and importance of the cathode and anode dimensions were clarified. To achieve preferential small fiber activation, a high current density in the epidermal skin layer is essential. The current density in the superficial skin layers increases as the dimensions of the cathode decrease, and thereby minimizing the cathode size will decrease the activation threshold of small fibers and increase preferential activation. A specific anode design is not necessary for preferential activation of small fibers as the anode dimensions have a limited effect on small fiber activation. Nevertheless, to improve preferential small fiber activation or perhaps even achieve selective small fiber activation, the anode is of high importance. Small anode-cathode distances and small anode areas help limit the current spread and thereby avoid contaminant activation of large non-nociceptive nerve fibers. By minimizing the electrode dimensions, a planar electrode design could potentially perform as well as intra-epidermal electrode designs.

Based on the results of study II a novel planar concentric array electrode was designed. The electrode consisted of seven interconnected concentric anode-cathode pairs. The electrode had a planar design and was printed on flexible plastic material, enabling electrode placement at any body part. Study III provided the initial exploration of the electrode and its performance. Evoked potentials revealed a bilateral origin and slightly longer latencies for the novel electrode design compared to a conventional patch configuration. Furthermore, reaction times for the novel planar concentric array electrode were longer, and the stimulus quality was described as sharp rather than dull. The sharpness and the intensity of the sensation increased with increasing stimulation intensity and may indicate that the electrode can be used for high-intensity stimulation of the nociceptive system.

## 5.2. FUTURE PERSPECTIVES

Study III was the initial exploration of the novel electrode design, and further studies to confirm and further evaluate electrode performance are needed. Such studies may include blockage of small fibers by either the application of topical lidocaine or pressure blocking. Furthermore, it could be interesting to use capsaicin application as a model for small fiber denervation. Such denervation of the nerves has previously been performed to confirm preferential small fiber activation [29], [41], and in combination with skin biopsies, it could also verify the model predictions of the nerve fiber termination depths for which an electrode design is small fiber preferential.

The novel electrode developed during this Ph.D. project was designed to improve preferential activation of small fibers and thereby increase the range of feasible stimulation intensities. Consequently, the electrode may be used to follow disease progression and patient outcome in small fiber neuropathy. In small fiber neuropathy, the small epidermal nerve fibers degenerate and retract, why higher currents would be necessary to activate them and assess fiber function. The membrane properties of small nerve fibers may be assessed through estimates of perception thresholds to different pulse shapes and durations [42], and this technique is expected to enable valuable investigation into the mechanism of neuropathy and neuropathic pain [47]. Previous studies using this technique have used the pin electrode. However, the novel planar concentric electrode may be an improvement to the method, both in relation to small fiber preferentiality but also to the applicability of the electrode in patient studies. Diabetic neuropathy is typically length-dependent, and therefore, nerve fiber assessments are often performed at the ankle joint. The pin electrode is not easily placed in this position due to its size, while the novel planar array electrode can be easily placed at any desired body location. Additionally, the pin electrode needs cleaning after each trial, whereas the novel planar concentric array electrode is a single-use disposable electrode.

The possibility to preferentially activate small fibers for high stimulation intensities furthermore expands the possible applications of the electrode in other areas of pain research. For example, high-frequency and high-intensity stimulation is used to induce long-term potentiation as a human pain model of secondary hyperalgesia [18]. For this pain model, intense activation of nociceptors is necessary and preferably without concomitant activation of non-nociceptive fibers [174], [175]. Improved preferential activation of small fibers would thus be of value in the investigation of secondary hyperalgesia as well as general neuroplasticity mechanism in pain models and chronic pain conditions.

Improved electrode designs for small fiber activation may be combined with special pulse shapes to further increase the preferential activation of small fibers. Hugosdottir et al. [26] showed that a bounded exponential pulse shape increased the difference between perception thresholds for large fiber and small-fiber preferential electrodes.



Furthermore, cathodal and anodal triangular pulses have been suggested for selective activation of A $\delta$ -fiber and C-fibers [28]. The computational model and the computational framework implemented in this project could be a valuable tool in the development and optimization of such stimulation pulses and entire protocols for small fiber assessment.

## LITERATURE LIST

- [1] Peters, M. J. H., Bakkers, M., Merkies, I. S. J., Hoeijmakers, J. G. J., van Raak, E., and Faber, C. G., 2013, Incidence and prevalence of small-fiber neuropathy, *Neurology*, **81**, 1356–1360.
- [2] Sopacua, M., Hoeijmakers, J. G. J., Merkies, I. S. J., Lauria, G., Waxman, S. G., and Faber, C. G., 2019, Small-fiber neuropathy: Expanding the clinical pain universe, 19–33.
- [3] Bakkers, M., Faber, C. G., Hoeijmakers, J. G. J., Lauria, G., and Merkies, I. S. J., 2014, Small fibers, large impact: Quality of life in small-fiber neuropathy, *Muscle and Nerve*, **49**, 329–336.
- [4] Attal, N., Lanteri-Minet, M., Laurent, B., Fermanian, J., and Bouhassira, D., 2011, The specific disease burden of neuropathic pain: Results of a French nationwide survey, *Pain*, **152**, 2836–2843.
- [5] Sharififar, S., Shuster, J. J., and Bishop, M. D., 2018, Adding electrical stimulation during standard rehabilitation after stroke to improve motor function. A systematic review and meta-analysis, *Ann. Phys. Rehabil. Med.*, **61**, 339–344.
- [6] Kwong, P. W. H., Ng, G. Y. F., Chung, R. C. K., and Ng, S. S. M., 2018, Transcutaneous electrical nerve stimulation improves walking capacity and reduces spasticity in stroke survivors: a systematic review and meta-analysis, *Clin. Rehabil.*, **32**, 1203–1219.
- [7] Vance, C. G. T., Dailey, D. L., Rakel, B. A., and Sluka, K. A., 2014, Using TENS for pain control: the state of the evidence, *Pain Manag.*, **4**, 197–209.
- [8] Mainka, T., Maier, C., and Enax-Krumova, E. K., 2015, Neuropathic pain assessment: Update on laboratory diagnostic tools, *Curr. Opin. Anaesthesiol.*, **28**, 537–545.
- [9] Baron, R. *et al.*, 2017, Peripheral neuropathic pain: a mechanism-related organizing principle based on sensory profiles, **158**.
- [10] Katsarava, Z., Yaldizli, Ö., Voulkoudis, C., Diener, H.-C., Kaube, H., and Maschke, M., 2006, Pain related potentials by electrical stimulation of skin for detection of small-fiber neuropathy in HIV, *J. Neurol.*, **253**, 1581–1584.
- [11] Suzuki, C., Kon, T., Funamizu, Y., Ueno, T., Haga, R., Nishijima, H., Arai, A., Tomiyama, M., and Baba, M., 2016, Elevated pain threshold in patients

- with asymptomatic diabetic neuropathy: an intraepidermal electrical stimulation study, *Muscle and Nerve*, **54**, 146–149.
- [12] Krarup, C., 2003, An update on electrophysiological studies in neuropathy, *Curr. Opin. Neurol.*, **16**, 603–612.
- [13] Bromm, B. and Meier, W., 1984, The Intracutaneous Stimulus: A New Pain Model for Algesimetric Studies, *Methods Find. Exp. Clin. Pharmacol.*, **6**, 405–410.
- [14] Inui, K., Tran, T. D., Hoshiyama, M., and Kakigi, R., 2002, Preferential stimulation of A $\delta$  fibers by intra-epidermal needle electrode in humans, *Pain*, **96**, 247–252.
- [15] Kaube, H., Katsarava, Z., Käufer, T., Diener, H.-C., and Ellrich, J., 2000, A new method to increase nociception specificity of the human blink reflex, *Clin. Neurophysiol.*, **111**, 413–416.
- [16] Steenbergen, P., Buitenweg, J. R., Trojan, J., van der Heide, E. M., van den Heuvel, T., Flor, H., and Veltink, P. H., 2012, A system for inducing concurrent tactile and nociceptive sensations at the same site using electrocutaneous stimulation., *Behav. Res. Methods*, **44**, 924–33.
- [17] Leandri, M., Marinelli, L., Siri, A., and Pellegrino, L., 2018, Micropatterned surface electrode for massive selective stimulation of intraepidermal nociceptive fibres, *J. Neurosci. Methods*, **293**, 17–26.
- [18] Klein, T., Margerl, W., Hopf, H.-C., Sandkühler, J., and Treede, R.-D., 2004, Perceptual Correlates of Nociceptive Long-Term Potentiation and Long-Term Depression in Humans, *J. Neurosci.*, **24**, 964–971.
- [19] Hugosdottir, R., Mørch, C. D., Jørgensen, C. K., Nielsen, C. W., Olsen, M. V., Pedersen, M. J., and Tigerholm, J., 2019, Altered excitability of small cutaneous nerve fibers during cooling assessed with the perception threshold tracking technique, *BMC Neurosci.*, **20**, 1–13.
- [20] Mørch, C. D., Hennings, K., and Andersen, O. K., 2011, Estimating nerve excitation thresholds to cutaneous electrical stimulation by finite element modeling combined with a stochastic branching nerve fiber model, *Med. Biol. Eng. Comput.*, **49**, 385–395.
- [21] Poulsen, A. H., Tigerholm, J., Meijs, S., Andersen, O. K., and Mørch, C. D., 2020, Comparison of existing electrode designs for preferential activation of cutaneous nociceptors, *J. Neural Eng.*, **17**.

- [22] Provitera, V., Nolano, M., Pagano, A., Caporaso, G., Stancanelli, A., and Santoro, L., 2007, Myelinated nerve endings in human skin, *Muscle Nerve*, **35**, 767–775.
- [23] Ebenezer, G. J., Hauer, P., Gibbons, C., McArthur, J. C., and Polydefkis, M., 2007, Assessment of epidermal nerve fibers: a new diagnostic and predictive tool for peripheral neuropathies., *J. Neuropathol. Exp. Neurol.*, **66**, 1059–1073.
- [24] Poulsen, A. H., Tigerholm, J., Andersen, O. K., and Mørch, C. D., 2021, Increased preferential activation of small cutaneous nerve fibers by optimization of electrode design parameters, *J. Neural Eng.*, **18**, 016020.
- [25] Lelic, D., Mørch, C. D., Hennings, K., Andersen, O. K., and Drewes, A. M., 2012, Differences in perception and brain activation following stimulation by large versus small area cutaneous surface electrodes, *Eur. J. Pain*, **16**, 827–837.
- [26] Hugosdottir, R., Mørch, C. D., Andersen, O. K., Helgason, T., and Arendt-Nielsen, L., 2019, Preferential activation of small cutaneous fibers through small pin electrode also depends on the shape of a long duration electrical current, *BMC Neurosci.*, **20**.
- [27] Otsuru, N., Inui, K., Yamashiro, K., Miyazaki, T., Osawa, I., Takeshima, Y., and Kakigi, R., 2009, Selective Stimulation of C Fibers by an Intra-Epidermal Needle Electrode in Humans, *Open Pain J.*, **2**, 53–56.
- [28] Kodaira, M., Inui, K., and Kakigi, R., 2014, Evaluation of nociceptive A $\delta$ - and C-fiber dysfunction with lidocaine using intraepidermal electrical stimulation, *Clin. Neurophysiol.*, **125**, 1870–1877.
- [29] Mouraux, A., Iannetti, G. D., and Plaghki, L., 2010, Low intensity intra-epidermal electrical stimulation can activate A $\delta$ -nociceptors selectively, *Pain*, **150**, 199–207.
- [30] Lefaucheur, J. P., Ahdab, R., Ayache, S. S., Lefaucheur-Ménard, I., Rouie, D., Tebbal, D., Neves, D. O., and Ciampi de Andrade, D., 2012, Pain-related evoked potentials: A comparative study between electrical stimulation using a concentric planar electrode and laser stimulation using a CO 2 laser, *Neurophysiol. Clin.*, **42**, 199–206.
- [31] Katsarava, Z., Ayzenberg, I., Sack, F., Limmroth, V., Diener, H. C., and Kaube, H., 2006, A novel method of eliciting pain-related potentials by transcutaneous electrical stimulation, *Headache*, **46**, 1511–1517.

- [32] Mouraux, A., Marot, E., and Legrain, V., 2014, Short trains of intra-epidermal electrical stimulation to elicit reliable behavioral and electrophysiological responses to the selective activation of nociceptors in humans, *Neurosci. Lett.*, **561**, 69–73.
- [33] Otsuru, N., Inui, K., Yamashiro, K., Miyazaki, T., Takeshima, Y., and Kakigi, R., 2010, Assessing A $\delta$  Fiber Function With Lidocaine Using Intraepidermal Electrical Stimulation, *J. Pain*, **11**, 621–627.
- [34] Omori, S., Iose, S., Misawa, S., Watanabe, K., Sekiguchi, Y., Shibuya, K., Beppu, M., Amino, H., and Kuwabara, S., 2017, Pain-related evoked potentials after intraepidermal electrical stimulation to A $\delta$  and C fibers in patients with neuropathic pain, *Neurosci. Res.*, **121**, 43–48.
- [35] Mueller, D., Obermann, M., Koeppen, S., Kavuk, I., Yoon, M.-S., Sack, F., Diener, H.-C., Kaube, H., and Katsarava, Z., 2010, Electrically evoked nociceptive potentials for early detection of diabetic small-fiber neuropathy, *Eur. J. Neurol.*, **17**, 834–841.
- [36] Kukidome, D. *et al.*, 2016, Measurement of small fibre pain threshold values for the early detection of diabetic polyneuropathy, *Diabet. Med.*, **33**, 62–69.
- [37] Yoon, M. S., Obermann, M., Dockweiler, C., Assert, R., Canbay, A., Haag, S., Gerken, G., Diener, H.-C., and Katsarava, Z., 2011, Sensory neuropathy in patients with cryoglobulin negative hepatitis-C infection, *J. Neurol.*, **258**, 80–88.
- [38] Obermann, M. *et al.*, 2008, Correlation of epidermal nerve fiber density with pain-related evoked potentials in HIV neuropathy, *Pain*, **138**, 79–86.
- [39] Perchet, C., Frot, M., Charmarty, A., Flores, C., Mazza, S., Magnin, M., and Garcia-Larrea, L., 2012, Do we activate specifically somatosensory thin fibres with the concentric planar electrode? A scalp and intracranial EEG study, *Pain*, **153**, 1244–1252.
- [40] de Tommaso, M., Santostasi, R., Devitofrancesco, V., Franco, G., Vecchio, E., Delussi, M., Livrea, P., and Katsarava, Z., 2011, A comparative study of cortical responses evoked by transcutaneous electrical vs CO<sub>2</sub> laser stimulation, *Clin. Neurophysiol.*, **122**, 2482–2487.
- [41] La Cesa, S. *et al.*, 2018, Skin denervation does not alter cortical potentials to surface concentric electrode stimulation: A comparison with laser evoked potentials and contact heat evoked potentials, *Eur. J. Pain*, **22**, 161–169.

- [42] Hennings, K., Frahm, K. S., Petrini, L., Andersen, O. K., Arendt-Nielsen, L., and Mørch, C. D., 2017, Membrane properties in small cutaneous nerve fibers in humans, *Muscle Nerve*, **55**, 195–201.
- [43] Di Stefano, G. *et al.*, 2020, The new micropatterned interdigitated electrode for selective assessment of the nociceptive system, *Eur. J. Pain (United Kingdom)*, **24**, 956–966.
- [44] Kalkman, R. K., Briaire, J. J., and Frijns, J. H. M., 2015, Current focussing in cochlear implants: An analysis of neural recruitment in a computational model, *Hear. Res.*, **322**, 89–98.
- [45] El-Negamy, E. and Sedgwick, E. M., 1978, Properties of a spinal somatosensory evoked potential recorded in man, *J. Neurol. Neurosurg. Psychiatry*, **41**, 762–768.
- [46] Tigerholm, J., Poulsen, A. H., Andersen, O. K., and Mørch, C. D., 2019, From Perception Threshold to Ion Channels—A Computational Study, *Biophys. J.*, **117**.
- [47] Tigerholm, J., Hoberg, T. N., Brønnum, D., Vittinghus, M., Frahm, K. S., and Mørch, C. D., 2020, Small and large cutaneous fibers display different excitability properties to slowly increasing ramp pulses, *J. Neurophysiol.*, **124**, 883–8894.
- [48] Mcneal, D. R., 1976, Analysis of a model for excitation of myelinated nerve, *IEEE Trans. Biomed. Eng.*, **BME-23**, 329–337.
- [49] Rattay, F., 1988, Modeling the excitation of fibers under surface electrodes, *IEEE Trans. Biomed. Eng.*, **35**, 199–202.
- [50] Hirata, A., Hattori, J., Laakso, I., Takagi, A., and Shimada, T., 2013, Computation of induced electric field for the sacral nerve activation, *Phys. Med. Biol.*, **58**, 7745–7755.
- [51] Motogi, J., Sugiyama, Y., Laakso, I., Hirata, A., Inui, K., Tamura, M., and Muragaki, Y., 2016, Why intra-epidermal electrical stimulation achieves stimulation of small fibres selectively: a simulation study, *Phys. Med. Biol.*, **61**, 4479–4490.
- [52] Sha, N., Kenney, L. P. J., Heller, B. W., Barker, A. T., Howard, D., and Moatamedi, M., 2008, A Finite Element Model to Identify Electrode Influence on Current Distribution in the Skin, *Artif. Organs*, **32**, 639–643.

- [53] Frahm, K. S., Hennings, K., Vera-Portocarrero, L., Wacnik, P. W., and Mørch, C. D., 2016, Nerve Fiber Activation during Peripheral Nerve Field Stimulation: Importance of Electrode Orientation and Estimation of Area of Paresthesia, *Neuromodulation*, **19**, 311–318.
- [54] Hart, F. X., 1992, Numerical and analytical methods to determine the current density distributions produced in human and rat models by electric and magnetic fields, *Bioelectromagn. Suppl.*, **13**, 27–42.
- [55] Andreuccetti, D. and Zoppetti, N., 2006, Quasi-static electromagnetic dosimetry: From basic principles to examples of applications, *Int. J. Occup. Saf. Ergon.*, **12**, 201–215.
- [56] Rattay, F., 1989, Analysis of Models for Extracellular Fiber Stimulation, *IEEE Trans. Biomed. Eng.*, **36**, 676–682.
- [57] Howell, B., Medina, L. E., and Grill, W. M., 2015, Effects of frequency-dependent membrane capacitance on neural excitability, *J. Neural Eng.*, **12**, 1–17.
- [58] Tigerholm, J., Petersson, M. E., Obreja, O., Lampert, A., Carr, R., Schmelz, M., and Fransén, E., 2014, Modeling activity-dependent changes of axonal spike conduction in primary afferent C-nociceptors., *J. Neurophysiol.*, **111**, 1721–35.
- [59] Carnevale, T. and Hines, M., *The NEURON Book*. Cambridge University Press, 2006.
- [60] Martini, F. H., Nath, J. L., and Bartholomew, E. F., The integumentary system, in *Fundamentals of Anatomy & physiology*, 2012, 144–168.
- [61] Nolano, M., Provitera, V., Crisci, C., Stancanelli, A., Wendelschafer-Crabb, G., Kennedy, W. R., and Santoro, L., 2003, Quantification of myelinated endings and mechanoreceptors in human digital skin, *Ann. Neurol.*, **54**, 197–205.
- [62] McArthur, J. C., Stocks, E. A., Hauer, P., Cornblath, D. R., and Griffin, J. W., 1998, Epidermal Nerve Fiber Density, *Arch. Neurol.*, **55**, 1513.
- [63] Kelly, E. J., Terenghi, G., Hazari, A., and Wiberg, M., 2005, Nerve fibre and sensory end organ density in the epidermis and papillary dermis of the human hand, *Br. J. Plast. Surg.*, **58**, 774–779.
- [64] Limbert, G., 2017, Mathematical and computational modelling of skin

- biophysics: A review, *Proc. R. Soc. A Math. Phys. Eng. Sci.*, **473**.
- [65] Benson, H. A. E. and Watkinson, A. C., Skin Structure, Function, and Permeation, in *Topical and Transdermal Drug delivery: Principles and practice*, Wiley, 2012, 3–22.
- [66] Sandby-Møller, J., Poulsen, T., and Wulf, H. C., 2003, Epidermal Thickness at Different Body Sites: Relationship to Age, Gender, Pigmentation, Blood Content, Skin Type and Smoking Habits, *Acta Derm. Venereol.*, **83**, 410–413.
- [67] Egawa, M., Hirao, T., and Takahashi, M., 2007, In vivo estimation of stratum corneum thickness from water concentration profiles obtained with raman spectroscopy, *Acta Derm. Venereol.*, **87**, 4–8.
- [68] Neerken, S., Lucassen, G. W., Bisschop, M. a., Lenderink, E., and Nuijs, T. (a. M. ., 2004, Characterization of age-related effects in human skin: A comparative study that applies confocal laser scanning microscopy and optical coherence tomography, *J. Biomed. Opt.*, **9**, 274.
- [69] Rajadhyaksha, M., González, S., Zavislan, J. M., Anderson, R. R., and Webb, R. H., 1999, In vivo confocal scanning laser microscopy of human skin II: Advances in instrumentation and comparison with histology, *J. Invest. Dermatol.*, **113**, 293–303.
- [70] Valentin, J., 2002, Basic anatomical and physiological data for use in radiological protection: reference values, *Ann. ICRP*, **32**, 1–277.
- [71] Huzaira, M., Rius, F., Rajadhyaksha, M., Anderson, R. R., and González, S., 2001, Topographic variations in normal skin, as viewed by in vivo reflectance confocal microscopy, *J. Invest. Dermatol.*, **116**, 846–852.
- [72] Alekseev, S. I. and Ziskin, M. C., 2007, Human skin permittivity determined by millimeter wave reflection measurements, *Bioelectromagnetics*, **28**, 331–339.
- [73] Krackowizer, P. and Brenner, E., 2008, Dicke der Epidermis und Dermis\* sonographische Messung an 24 Stellen des Menschlichen Körpers, *Phlebologie*, **37**, 83–92.
- [74] Arthur, R. P. and Shelley, W. B., 1959, The Innervation of Human Epidermis, *J. Invest. Dermatol.*, **32**, 397–411.
- [75] Kandel, E. R., Schwartz, J. H., and Jessell, T. M., The bodily Senses, in *Principles of neural science*, 4th ed., McGraw-Hill, 2000, 430–450.



- [76] Ringkamp, T., Raja, S. N., Campbell, J. N., and Meyer, R. A., Peripheral Mechanisms of Cutaneous Nociception, in *Neurobiology of Pain*, 1–30.
- [77] Millan, M. J., 1999, The induction of pain: An integrative review, *Prog. Neurobiol.*, **57**, 1–164.
- [78] Schwan, H. P., 1968, Electrical impedance of the human body.
- [79] Pethig R., 1984, Dielectric Properties of Biological Materials: Biophysical and Medical Applications, *IEEE T Electr Insul*, **EI-19**, 453–474.
- [80] Pethig, R., 1987, Dielectric properties of body tissues, *Clin. Phys. Physiol. Meas.*, **8**, 5–12.
- [81] Marzec, E. and Wachal, K., 1999, The electrical properties of leg skin in normal individuals and in patients with ischemia, *Bioelectrochemistry Bioenerg.*, **49**, 73–75.
- [82] Nasir, N. and Ahmad, M. Al., 2020, Cells Electrical Characterization: Dielectric Properties, Mixture, and Modeling Theories, *J. Eng.*, **2020**, 1–17.
- [83] Schwan, H. P. and Foster, K. R., 1980, RF-field interactions with biological systems: Electrical properties and biophysical mechanisms, *Proc. IEEE*, **68**, 104–113.
- [84] Grimnes, S., 1983, Skin impedance and electro-osmosis in the human epidermis, *Med. Biol. Eng. Comput.*, **21**, 739–749.
- [85] Mc Rae, D. A. and Esrick, M. A., 1993, Changes in electrical impedance of skeletal muscle measured during hyperthermia, *Int. J. Hyperth.*, **9**, 247–261.
- [86] Faes, T., Van der Meij, H., de Munck, J., and Heethaar, R., 1999, The electric resistivity of human tissues ( 100 Hz-10 MHz ): a meta-analysis of review studies, *Physiol. Meas.*, **20**, R1–R10.
- [87] Eggins, B. R., 1993, Skin contact electrodes for medical applications, *Analyst*, **4**, 439–442.
- [88] Yamamoto, T. and Yamamoto, Y., 1976, Electrical properties of the epidermal stratum corneum, *Med. Biol. Eng.*, **14**, 151–158.
- [89] Birgersson, U. H., Birgersson, E., and Ollmar, S., 2012, Estimating electrical properties and the thickness of skin with electrical impedance spectroscopy: Mathematical analysis and measurements, *J. Electr. Bioimpedance*, **3**, 51–60.

- [90] Gabriel, S., Lau, R. W., and Gabriel, C., 1996, The dielectric properties of biological tissues: III. Parametric models for the dielectric spectrum of tissues, *Phys. Med. Biol.*, **41**, 2271–2293.
- [91] Tavernier, A., Dierickx, M., and Hinsenkamp, M., 1993, Tensors of dielectric permittivity and conductivity of in vitro human derms and epiderms., *Bioelectroch. Bioener.*, **30**, 65–72.
- [92] Gabriel, S., Gabriel, C., and W, L. R., 1996, The dielectric properties of biological tissues: II. Measurements in the frequency range 10 Hz to 20 GHz, *Phys. Med. Biol.*, **41**, 2251–2260.
- [93] Gabriel, C., Gabriel, S., and Corthout, E., 1996, The dielectric properties of biological tissues: I. Literature survey, *Phys. Med. Biol.*, **41**, 2231–2249.
- [94] Martini, F. H., Bartholomew, E. F., and Nath, J. L., Neural Tissue, in *Fundamentals of Anatomy & Physiology*, 9th intern., Pearson, 2012, 374–396.
- [95] Mortimer, J. T. and Bhadra, N., *Fundamentals of Electrical Stimulation*, Volume 1., **1**. Elsevier Ltd, 2009.
- [96] Mogyoros, I., Kiernan, M. C., and Burke, D., 1996, Strength-duration properties of human peripheral nerve., *Brain*, **119**, 439–447.
- [97] Geddes, L. A. and Bourland, J. D., 1985, The Strength-Duration Curve, *IEEE Trans. Biomed. Eng.*, **32**, 458–459.
- [98] Hill, A. V., 1935, Excitation and Accomodation in Nerves, *Proceesings R. Soc. London, Biol. Sci.*, 305–355.
- [99] Böhling, A., Bielfeldt, S., Himmelmann, A., Keskin, M., and Wilhelm, K. P., 2014, Comparison of the stratum corneum thickness measured in vivo with confocal Raman spectroscopy and confocal reflectance microscopy, *Ski. Res. Technol.*, **20**, 50–57.
- [100] Moore, T. L., Lunt, M., McManus, B., Anderson, M. E., and Herrick, A. L., 2003, Seventeen-point dermal ultrasound scoring system - A reliable measure of skin thickness in patients with systemic sclerosis, *Rheumatology*, **42**, 1559–1563.
- [101] Andreuccetti, D., Fossi, R., and Petrucci, C., An internet resource for the calculation of the dielectric properties of the body tissues in the frequency range 10 Hz-100 GHz, *IFAC, Florence(Italy) - Based on data published by C. Gabriel et. al in 19, 1997.* [Online]. Available:

<http://niremf.ifac.cnr.it/tissprop/>.

- [102] Kuhn, A., Keller, T., Micera, S., and Morari, M., 2009, Array electrode design for transcutaneous electrical stimulation: A simulation study, *Med. Eng. Phys.*, **31**, 945–951.
- [103] Keller, T. and Kuhn, A., 2008, Electrodes for transcutaneous (surface) electrical stimulation, *J. Autom. Control*, **18**, 35–45.
- [104] Merrill, D. R., Bikson, M., and Jefferys, J. G. R., 2005, Electrical stimulation of excitable tissue: Design of efficacious and safe protocols, *J. Neurosci. Methods*, **141**, 171–198.
- [105] Geddes, L. A., 1997, Historical Evolution of Circuit Models for the Electrode-Electrolyte Interface, *Ann. Biomed. Eng.*, **25**, 1–14.
- [106] Joucla, S. and Yvert, B., 2012, Modeling extracellular electrical neural stimulation: From basic understanding to MEA-based applications, *J. Physiol. Paris*, **106**, 146–158.
- [107] Joucla, S., Glière, A., and Yvert, B., 2014, Current approaches to model extracellular electrical neural microstimulation, *Front. Comput. Neurosci.*, **8**, 1–12.
- [108] Chi, Y. M., Jung, T. P., and Cauwenberghs, G., 2010, Dry-contact and noncontact biopotential electrodes: Methodological review, *IEEE Rev. Biomed. Eng.*, **3**, 106–119.
- [109] Kuhn, A., Keller, T., Lawrence, M., and Morari, M., 2009, A model for transcutaneous current stimulation: Simulations and experiments, *Med. Biol. Eng. Comput.*, **47**, 279–289.
- [110] Pelot, N. A., Thio, B. J., and Grill, W. M., 2018, Modeling Current Sources for Neural Stimulation in COMSOL, *Front. Comput. Neurosci.*, **12**, 1–14.
- [111] Manual, P. R., 2010, COMSOL Multiphysics Programming Reference Manual.
- [112] Warman, E. N., Grill, W. M., and Durand, D., 1992, Modelling the Effect of Electric Field on Nerve Fibers: Determination of Excitation Threshold, *IEEE Trans. Biomed. Eng.*, **39**, 1244–1254.
- [113] Moffitt, M. A., McIntyre, C. C., and Grill, W. M., 2004, Prediction of Myelinated Nerve Fiber Stimulation Thresholds: Limitations of Linear

Models, *IEEE Trans. Biomed. Eng.*, **51**, 229–236.

- [114] Pelot, N. A., Catherall, D. C., Thio, B. J., Titus, N. D., Liang, E. D., Henriquez, C. S., and Grill, W. M., 2021, Excitation properties of computational models of unmyelinated peripheral axons, *J. Neurophysiol.*, **125**, 86–104.
- [115] Tranchina, D. and Nicholson, C., 1986, A model for the polarization of neurons by extrinsically applied electric fields, *Biophys. J.*, **50**, 1139–1156.
- [116] Barret, E. F. and Barret, J. N., 1982, Intracellular recording from vertebrate myelinated axons: mechanism of the depolarizing afterpotential, *J. Physiol.*, **323**, 117–144.
- [117] McIntyre, C. C., Richardson, A. G., and Grill, W. M., 2002, Modeling the Excitability of Mammalian Nerve Fibers: Influence of Afterpotentials on the Recovery Cycle, *J. Neurophysiol.*, **87**, 995–1006.
- [118] Burke, D., Kiernan, M. C., and Bostock, H., 2001, Excitability of human axons, *Clin. Neurophysiol.*, **112**, 1575–1585.
- [119] Zhou, L. and Chiu, S. Y., 2001, Computer Model for Action Potential Propagation Through Branch Point in Myelinated Nerves, *J. Neurophysiol.*, **85**, 197–210.
- [120] Bennett, D. L., Clark, A. J., Huang, J., Waxmann, S. G., and Dib-Hajj, S. D., 2019, The role of voltage-gated sodium channels in pain signalling, *Physiol. Rev.*, **99**, 1079–1151.
- [121] Rasband, M. N., Park, E. W., Vanderah, T. W., Lai, J., Porreca, F., and Trimmer, J. S., 2001, Distinct potassium channels on pain-sensing neurons, *Proc. Natl. Acad. Sci. U. S. A.*, **98**, 13373–13378.
- [122] Akopian, A. N., Sivilotti, L., and Wood, J. N., 1996, A tetrodotoxin-resistant voltage-gated sodium channel expressed by sensory neurons, *J. Physiol.*, **379**, 257–262.
- [123] Djouhri, L., Fang, X., Okuse, K., Wood, J., Berry, C., and SN, L., 2003, The TTX-resistant sodium channel Nav1.8(SNS/PN3): expression and correlation with membrane properties in rat nociceptive primary afferent neurons, *J. Physiol.*, **550**, 739–752.
- [124] Weidner, C., Schmidt, R., Schmelz, M., ToreBjörk, E., and Handwerker, H. O., 2003, Action potential conduction in the terminal arborisation of

- nociceptive C-fibre afferents, *J. Physiol.*, **547**, 931–940.
- [125] Hodgkin, A. L. and Huxley, A. F., 1952, A quantitative description of membrane current and its application to conduction and excitation in nerve, *J. Physiol.*, **117**, 500–544.
- [126] Cannon, R. C. and D’alessandro, G., 2006, The ion channel inverse problem: Neuroinformatics meets biophysics, *PLoS Comput. Biol.*, **2**, e91.
- [127] Andreozzi, E., Carannante, I., D’addio, G., Cesarelli, M., and Balbi, P., 2019, Phenomenological models of Nav1.5. A side by side, procedural, hands-on comparison between Hodgkin-Huxley and kinetic formalisms, *Sci. Rep.*, **9**.
- [128] Hugosdottir, R., Mørch, C. D., Andersen, O. K., and Arendt-Nielsen, L., 2019, Investigating stimulation parameters for preferential small-fiber activation using exponentially rising electrical currents, *J. Neurophysiol.*, **122**, 1745–1752.
- [129] Hoberg, T. N., Frahm, S., Hennings, K., Arendt-Nielsen, L., and Mørch, C. D., 2019, Assessing the modulation of cutaneous sensory fiber excitability using a fast perception threshold tracking technique, *Muscle Nerve*, 1–8.
- [130] Woo, E. J., Hua, P., Webster, J. G., Tompkins, W. J., and Pallás-Areny, R., 1992, Skin impedance measurements using simple and compound electrodes, *Med. Biol. Eng. Comput.*, **30**, 97–102.
- [131] C, L. J. D. M. and G., 1959, Electrical Characteristics of the skin, *J. Invest. Dermatol.*, **34**, 301–309.
- [132] Rosell, J., Colominas, J., Riu, P., Pallas-Areny, R., and Webster, J. G., 1988, Skin Impedance From 1 Hz to 1 MHz, *IEEE Trans. Biomed. Eng.*, **35**, 649–652.
- [133] Kuhn, A., Keller, T., Lawrence, M., and Morari, M., 2010, The Influence of Electrode Size on Selectivity and Comfort in Transcutaneous Electrical Stimulation of the Forearm, *IEEE Trans. Neural Syst. Rehabil. Eng.*, **18**, 255–262.
- [134] Luersen, M. A., Le Riche, R., and Guyon, F., 2004, A constrained, globalized, and bounded Nelder-Mead method for engineering optimization, *Struct. Multidiscip. Optim.*, **27**, 43–54.
- [135] Barton, R. R. and Ivey, J. S., 1996, Nelder-Mead Simplex Modifications for Simulation Optimization, **42**, 954–973.

- [136] Gosavi, A., Parametric Optimization: Stochastic Gradients and Adaptive Search, in *Simulation-Based Optimization, Parametric Optimization Techniques and Reinforcement Learning*, 2015, 71–122.
- [137] Inui, K. and Kakigi, R., 2012, Pain perception in humans: use of intraepidermal electrical stimulation, *J. Neurol. Neurosurg. Psychiatry*, **83**, 551–556.
- [138] Pittenger, G. L., Ray, M., Burcus, N. I., McNulty, P., Basta, B., and Vinik, A. I., 2004, Intraepidermal Nerve Fibers Are Indicators of Small-Fiber Neuropathy in Both Diabetic and Nondiabetic Patients, *Diabetes Care*, **27**, 1974–1979.
- [139] Karlsson, P., Hincker, A. M., Jensen, T. S., Freeman, R., and Haroutounian, S., 2019, Structural, functional, and symptom relations in painful distal symmetric polyneuropathies: a systematic review, *Pain*, **160**, 286–297.
- [140] Lowery, M. M., Stoykov, N. S., Dewald, J. P. A., and Kuiken, T. A., 2004, Volume conduction in an anatomically based surface EMG model, *IEEE Trans. Biomed. Eng.*, **51**, 2138–2147.
- [141] Taylor, N. A. S. and Machado-Moreira, C. A., 2013, Regional variations in transepidermal water loss, eccrine sweat gland density, sweat secretion rates and electrolyte composition in resting and exercising humans, *Extrem. Physiol. Med.*, **2**, 1.
- [142] Chizmadzhev, Y. A., Indenbom, A. V., Kuzmin, P. I., Galichenko, S. V., Weaver, J. C., and Potts, R. O., 1998, Electrical properties of skin at moderate voltages: Contribution of appendageal macropores, *Biophys. J.*, **74**, 843–856.
- [143] Demonte, T. P., Patriciu, A., Joy, M. L. G., and Struijk, J. J., 2001, Current Densities Produced by Surface Electrodes: Comparison of MRI measurements and Finite Element, *Proc. Intl. Soc. Mag. Reson. Med*, **9**, 2001.
- [144] Patriciu, A., DeMonte, T. P., Joy, M. L. ., and Struijk, J. J., 2001, Investigation of current densities produced by surface electrodes using finite element modeling and current density imaging, *Eng. Med. Biol. Soc. 2001. Proc. 23rd Annu. Int. Conf. IEEE*, **3**, 2403–2406.
- [145] Joy, M. L. G., 2004, MR current density and conductivity imaging: The state of the art, *Annu. Int. Conf. IEEE Eng. Med. Biol. - Proc.*, **26 VII**, 5315–5319.
- [146] Vargas Luna, J. L., Krenn, M., Cortés Ramírez, J. A., and Mayr, W., 2015, Dynamic impedance model of the skin-electrode interface for transcutaneous

- electrical stimulation, *PLoS One*, **10**, 1–15.
- [147] Kiernan, M. C. *et al.*, 2020, Measurement of axonal excitability: Consensus guidelines, *Clin. Neurophysiol.*, **131**, 308–323.
- [148] Parker, J. L., Shariati, N. H., and Karantonis, D. M., 2018, Electrically evoked compound action potential recording in peripheral nerves, *Bioelectron. Med.*, **1**, 71–83.
- [149] Bostock, H., Cikurel, K., and Burke, D., 1998, Threshold tracking techniques in the study of human peripheral nerve, *Muscle and Nerve*, **21**, 137–158.
- [150] Geddes, L. A., 2004, Accuracy Limitations of Chronaxie Values, *IEEE T Bio-Med Eng*, **51**, 176–181.
- [151] Hennings, K., Frahm, K. S., Petrini, L., Andersen, O. K., Arendt-Nielsen, L., and Mørch, C. D., 2017, Membrane properties in small cutaneous nerve fibers, *Muscle Nerve*, **55**, 195–201.
- [152] Doll, R. J., van Amerongen, G., Hay, J. L., Groeneveld, G. J., Veltink, P. H., and Buitenweg, J. R., 2016, Responsiveness of electrical nociceptive detection thresholds to capsaicin (8 %)-induced changes in nociceptive processing, *Exp. Brain Res.*, **234**, 2505–2514.
- [153] Mogyoros, I., Kiernan, M. C., and Burke, D., 1996, Strength-duration properties of human peripheral nerve, *Brain*, **119**, 439–447.
- [154] Doll, R. J., Maten, A. C. A., Spaan, S. P. G., Veltink, P. H., and Buitenweg, J. R., 2016, Effect of temporal stimulus properties on the nociceptive detection probability using intra-epidermal electrical stimulation, *Exp. Brain Res.*, **234**, 219–227.
- [155] Russell, L. M., Wiedersberg, S., and Begoña Delgado-Charro, M., 2008, The determination of stratum corneum thickness An alternative approach, *Eur. J. Pharm. Biopharm.*, **69**, 861–870.
- [156] Cortex Technology ApS - Denmark. [Online]. Available: <http://www.cortex.dk/>. [Accessed: 24-May-2018].
- [157] Cruccu, G., Aminoff, M. J., Curio, G., Guerit, J. M., Kakigi, R., Mauguiere, F., Rossini, P. M., Treede, R. D., and Garcia-Larrea, L., 2008, Recommendations for the clinical use of somatosensory-evoked potentials, *Clin. Neurophysiol.*, **119**, 1705–1719.

- [158] Mouraux, A., De Paepe, A. L., Marot, E., Plaghki, L., Iannetti, G. D., and Legrain, V., 2013, Unmasking the obligatory components of nociceptive event-related brain potentials, *J. Neurophysiol.*, **110**, 2312–2324.
- [159] Kunde, V. and Treede, R. D., 1993, Topography of middle-latency somatosensory evoked potentials following painful laser stimuli and non-painful electrical stimuli, *Electroencephalogr. Clin. Neurophysiol. Evoked Potentials*, **88**, 280–289.
- [160] van den Berg, B., Doll, R. J., Mentink, A. L. H., Siebenga, P. S., Groeneveld, G. J., and Buitenweg, J. R., 2020, Simultaneous tracking of psychophysical detection thresholds and evoked potentials to study nociceptive processing, *Behav. Res. Methods*, **52**, 1617–1628.
- [161] Kida, T., Nishihira, Y., Wasaka, T., Sakajiri, Y., and Tazoe, T., 2004, Differential modulation of the short- and long-latency somatosensory evoked potentials in a forewarned reaction time task, *Clin. Neurophysiol.*, **115**, 2223–2230.
- [162] Berg, B. Van Den and Buitenweg, J. R., 2018, Analysis of Nociceptive Evoked Potentials during Multi-Stimulus Experiments using Linear Mixed Models, *40th Annu. Int. Conf. IEEE Eng. Med. Biol. Soc.*, 3048–3051.
- [163] Legrain, V., Mancini, F., Sambo, C. F., Torta, D. M., Ronga, I., and Valentini, E., 2012, Cognitive aspects of nociception and pain. Bridging neurophysiology with cognitive psychology, *Neurophysiol. Clin.*, **42**, 325–336.
- [164] Nagi, S. S. *et al.*, 2019, An ultrafast system for signaling mechanical pain in human skin, *Sci. Adv.*, **5**, 1–11.
- [165] Handwerker, H. O. and Kobal, G., 1993, Psychophysiology of experimentally induced pain, *Physiol. Rev.*, **73**, 639–671.
- [166] Melzack, R., 1999, From the gate to the neuromatrix, *Pain*, **pain suppl**, 121–126.
- [167] Félix, E. P. V, Giuliano, L. M. P., Tierra-Criollo, C. J., Gronich, G., Braga, N. I. O., Peres, C. A., Nóbrega, J. A. M., and Manzano, G. M., 2009, Sensations and reaction times evoked by electrical sinusoidal stimulation, *Neurophysiol. Clin.*, **39**, 283–290.
- [168] Kida, T., Nishihira, A. Y., and Hatta, A. A., 2003, Changes in the somatosensory N250 and P300 by the variation of reaction time, 326–330.



- [169] Lakhani, B., Vette, A. H., Mansfield, A., Miyasike-daSilva, V., and McIlroy, W. E., 2012, Electrophysiological Correlates of Changes in Reaction Time Based on Stimulus Intensity, *PLoS One*, **7**.
- [170] Campbell, J. N. and Lamotte, R. H., 1983, Latency to Detection of First Pain, *266*, 203–208.
- [171] Lele, P. P., Sinclair, D. C., and Weddell, G., 1954, The reaction time to touch, *J. Physiol.*, **123**, 187–203.
- [172] Teichner, W. H., 1954, Recent studies of simple reaction time, *Psychol. Bull.*, **51**, 128–149.
- [173] Pins, D. and Bonnet, C., 1996, On the relation between stimulus intensity and processing time: Piéron's law and choice reaction time, *Percept. Psychophys.*, **58**, 390–400.
- [174] Henrich, F., Magerl, W., Klein, T., Greffrath, W., and Treede, R. D., 2015, Capsaicin-sensitive C- and A-fibre nociceptors control long-term potentiation-like pain amplification in humans, *Brain*, **138**, 2505–2520.
- [175] Ziegler, E. A., Magerl, W., Meyer, R. A., and Treede, R., 1999, Secondary hyperalgesia to punctate mechanical stimuli Central sensitization to A-fibre nociceptor input, 2245–2257.



# LIST OF FIGURES

Figure 1.1: Outline of the Ph.D. dissertation.....18

Figure 2.1: Anatomy and structure of the skin. ....20

Figure 2.2: General schematic of the frequency dependencies of the permittivity and conductivity of living tissues. ....23

Figure 2.3: The routes of the current through the skin tissues. At low frequencies, the cell conducts poorly compared to the extracellular electrolyte and thus limits the current flow to the extracellular fluid. For higher frequencies around and above the frequency range of the  $\beta$ -dispersion, the cell membrane barrier breaks down, allowing the current to flow through the cells. The last route the current may take is through skin appendages, such as sweat ducts, that, when filled, provide a low impedance pathway for the current. ....24

Figure 2.4: Illustration of electrical surface stimulation of a peripheral nerve fiber axon. ....26

Figure 3.1: Implemented boundary conditions in the volume conduction model. ....37

Figure 3.2: Illustration of the nerve fiber models implemented in studies I and II. The models ran horizontally within the hypodermis before making a 45-degree bend towards the skin surface. The A $\beta$ -fiber model terminated within the dermis, while the A $\delta$ -fiber model continued into the epidermis. The myelin of the A $\delta$ -fiber model was lost as the fiber crossed the dermal-epidermal junction. Furthermore, the A $\delta$ -fiber model displayed two secondary branches with a 90-degree angle from the main branch. The nerve fiber models were single cable models, including the node, the juxtaparanode, and the internode. The figure is not drawn to scale. ....40

Figure 3.3: Illustration of the calculated area of selectivity. ....45

Figure 3.4: Flowchart of the procedure for determining the area of selectivity. ....45

Figure 3.5: Flowchart of the Globalized Bounded Nelder Mead (GBNM) algorithm used in study II [24]. Three runs were performed for each parameter with random initialization of the simplex. ....48

Figure 3.6: Illustration of the electrode parameters investigated In the optimization (study II) and the lower and upper bounds used to restrict the range of the solution space. Sketches of electrode parameters are modified from study II [24], and not drawn to scale. © IOP Publishing, reproduced with permission. All rights reserved. ....49

Figure 4.1: Activation threshold ratios between the two nerve fiber models at different dimensions of investigated electrode design parameters. Sketches of electrode parameters are modified from study II [24], and not drawn to scale. © IOP Publishing, reproduced with permission. All rights reserved. ....60

Figure 4.2: The nerve fiber activation threshold ratio between the two nerve fiber models as a function of the A $\delta$ -fiber termination depth. The stars indicate the sampled points. The dashed red line indicates nerve fiber preferentiality. Above the line, the A $\delta$ -fiber model achieved the lowest activation threshold. Below the line, the A $\beta$ -fiber model achieved a lower activation threshold than the A $\delta$ -fiber model. The activation

threshold ratio, as well as the depth for which preferential A $\delta$ -fiber activation was possible, was increased when electrode dimensions were optimized.....61

Figure 4.3: Novel planar concentric array electrode design. The electrode base was a flexible PET material on which silver layers were printed. Several insulating layers were added between the layers of the anode and cathodes to avoid shortcircuiting. The electrode consists of seven interconnected concentric cathode-anode pairs positioned in a hexagonal pattern. The cathodes had a diameter of 0.5 mm. The inner diameter of the anode was 1.53 mm, corresponding to an anode-cathode distance of 0.51 mm. The width of the anode was 0.31 mm, corresponding to an outer anode diameter of 2.14 mm. The distance between the outer border of the interconnected anodes was 1.28 mm. The entire electrode had a width of 9.94 mm and a total length of 35.36 mm. .63

Figure 4.4: The electrical potential underneath the center of the cathode, for electrode dimensions of the original planar concentric electrode and the novel planar concentric array electrode. ....64

Figure 4.5: Activation threshold of the two nerve fiber models for the original and the novel electrode design.....65

Figure 4.6: Strength-duration curves for the novel planar concentric array electrode, the planar concentric electrode, and the intra-epidermal electrode for a single subject and five repetitions. Data were obtained for a single subject with five repetitions for each of the electrodes, performed on five consecutive days. ....66

Figure 4.7: Average perception thresholds and standard errors for a 0.5 ms rectangular stimulation pulse for different electrode designs. Data on the Patch study I, Planar array, Planar concentric, Intra-epidermal, and Pin electrode are from study I, including 15 subjects. The data on the Patch study III and Planar concentric array electrodes were obtained in study III, containing data from 25 subjects. Electrode images of the patch, planar array, planar concentric, intra-epidermal and pin electrode are modified from study I [21]. © IOP Publishing, reproduced with permission. All rights reserved. ....70

Figure 4.8: Median reaction times and interquartile range for a rectangular stimulation pulse of 0.5 ms duration for different electrode designs. Data on the Patch study I, Planar array, Planar concentric, Intra-epidermal, and Pin electrode are from study I, including 15 subjects. The data on the Patch study III and Planar concentric array electrodes were obtained in study III, containing data from 25 subjects. Electrode images of the patch, planar array, planar concentric, intra-epidermal and pin electrode are modified from study I [21]. © IOP Publishing, reproduced with permission. All rights reserved.....71

## LIST OF TABLES

Table 2.1: Properties of different sensory nerve fibers [75]. .....	22
Table 3.1: Electrical properties of the implemented skin layers. The applied minimum and maximum values were used in the sensitivity analysis of the model [21], [24]. The model implemented values were used in the simulations investigating electrode designs in studies I and II. ....	32
Table 3.2: Chronaxie values for small and large fibers found in the literature. ....	56
Table 4.1: The original and optimized electrode dimensions and the resulting activation of the nerve fiber models. ....	60

ISSN (online): 2246-1302  
ISBN (online): 978-87-7210-957-2

**AALBORG UNIVERSITY PRESS**